Image Formation

Early Clinical SPECT

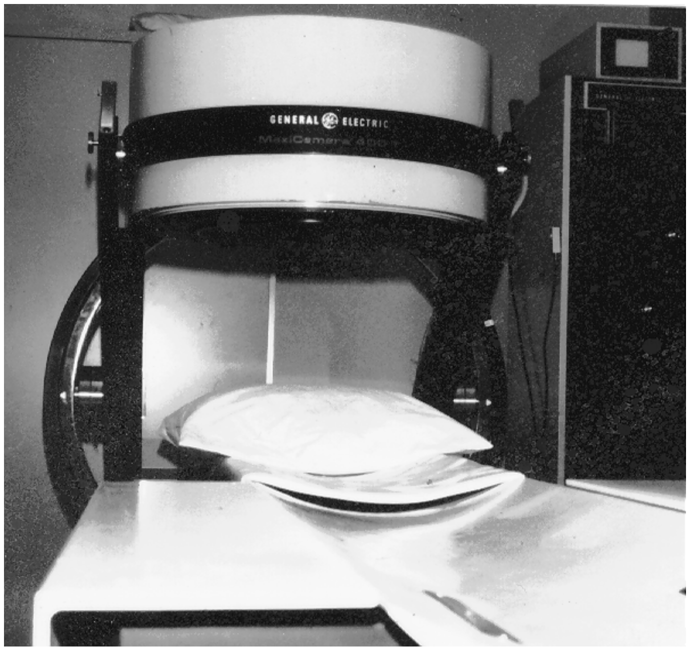

The First Anger Camera

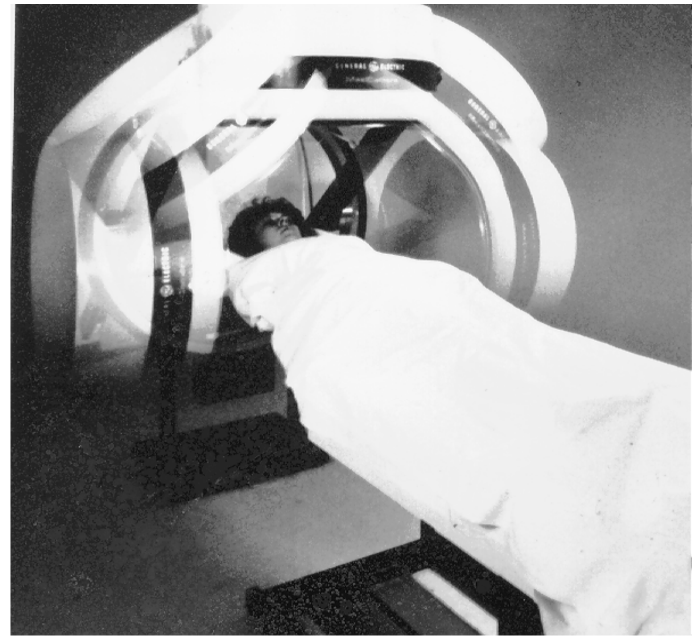

GE 400T Rotating Anger Camera (ca. 1981)

Modern Clinical Systems

GE Millenium VG

Philips Cardio 60

Siemens e.cam
Variable Angle

Basic SPECT – Projection Data

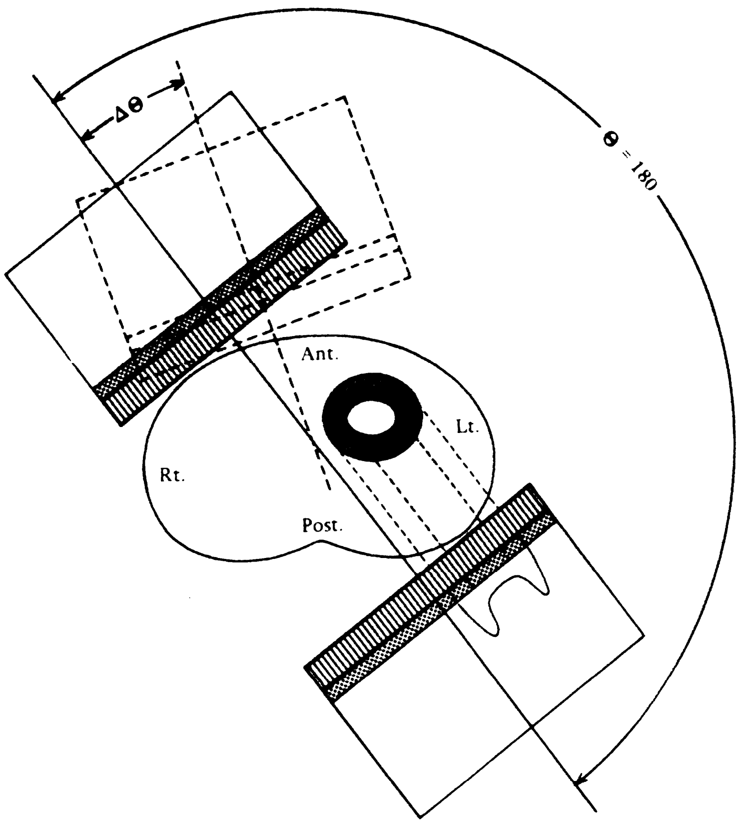

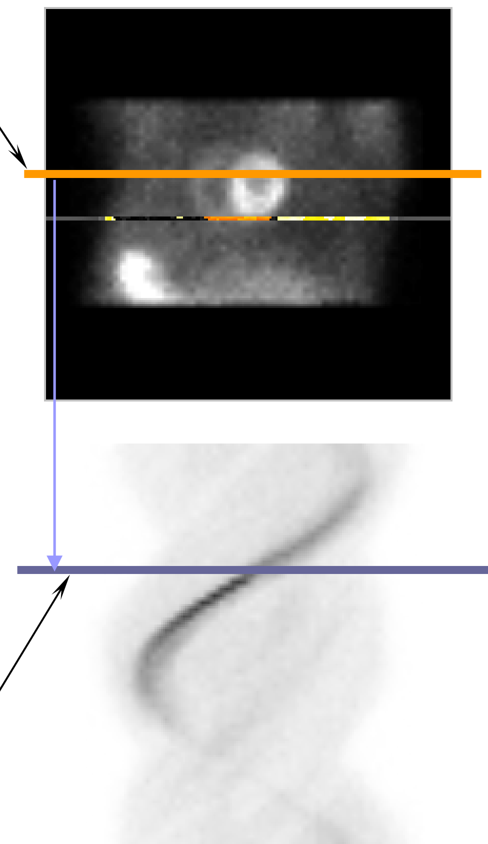

Collimation Systems

- The collimation system is the heart of the SPECT instrument – it's the front-end and has the biggest impact on SNR
- Its function is to form an image by determining the direction along which gamma-rays propagate
- Ideally, a lens similar to that used for visible photon wavelengths would be used for high efficiency – not feasible at gamma-ray wavelengths
- Absorbing collimation typically used

Pinhole Collimation

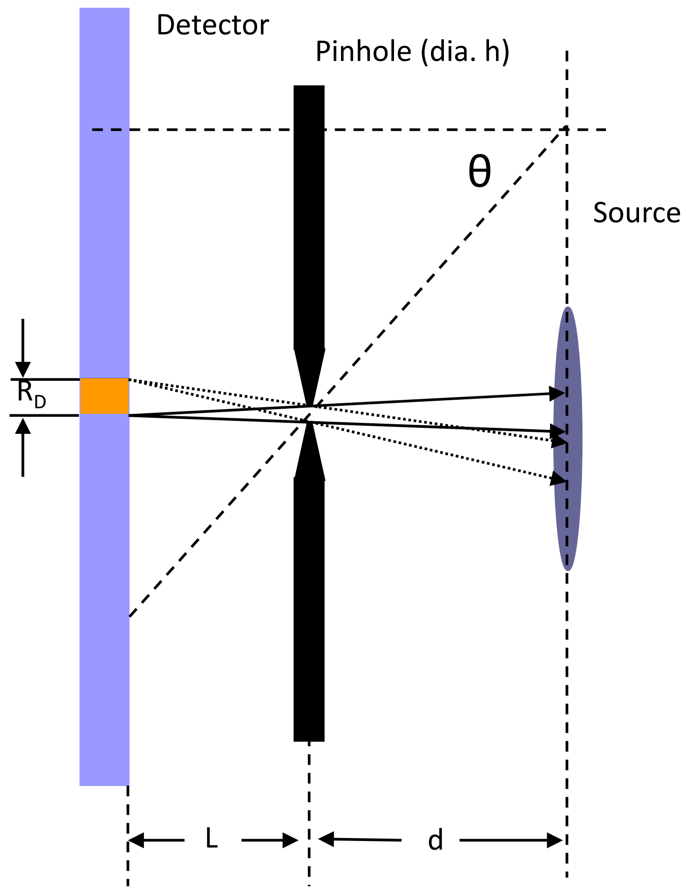

Intrinsic Resolution

$$R = h + \frac{h}{L} \times d$$

Efficiency

$$\eta < \frac{h^2}{16d^2} \cos^3\theta$$

Combined Resolution

$$R_{\text{Total}} \approx \sqrt{\left(R^2 + \left(\frac{d}{L} \times R_D \right)^2 \right)}$$

Parallel Hole Collimation

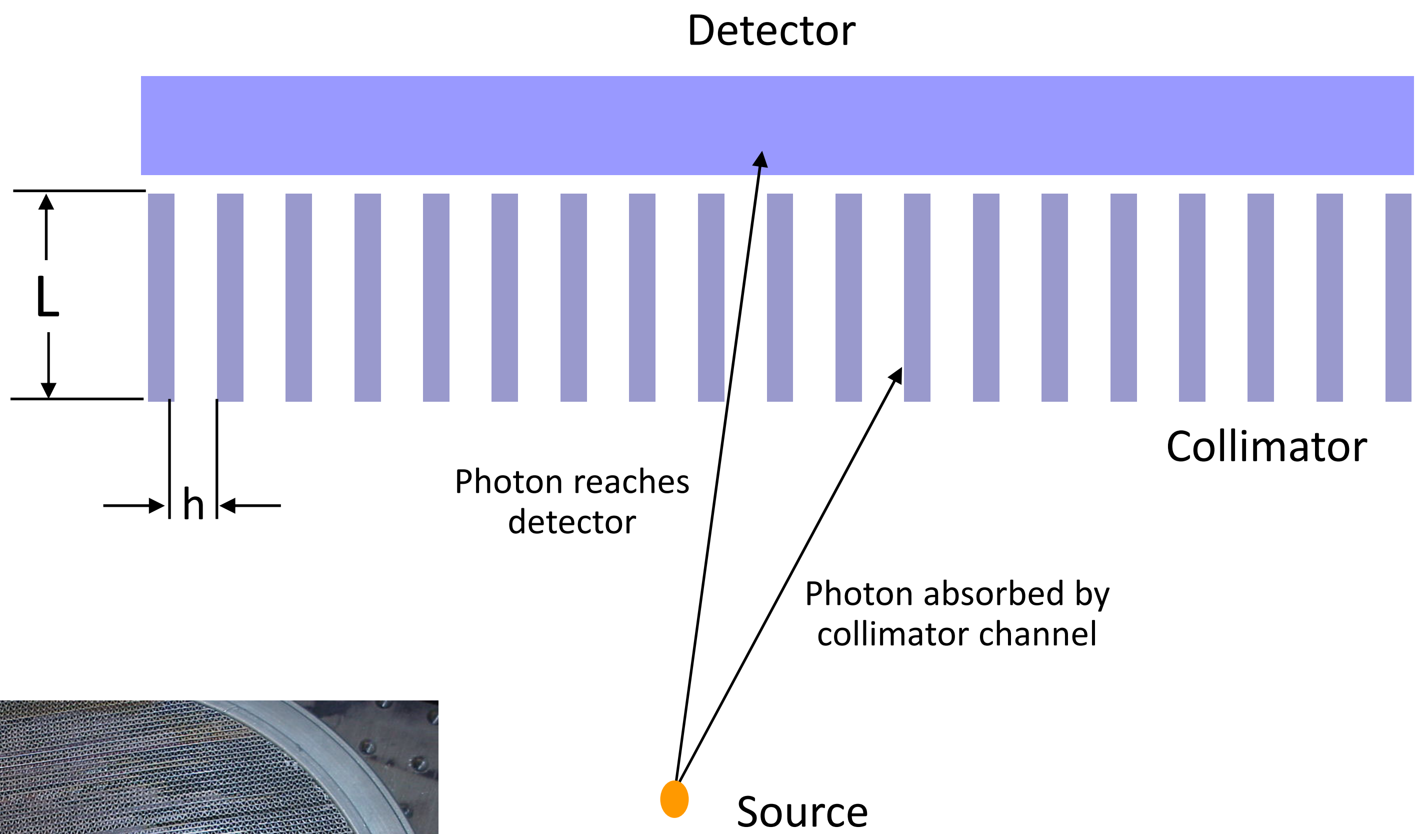

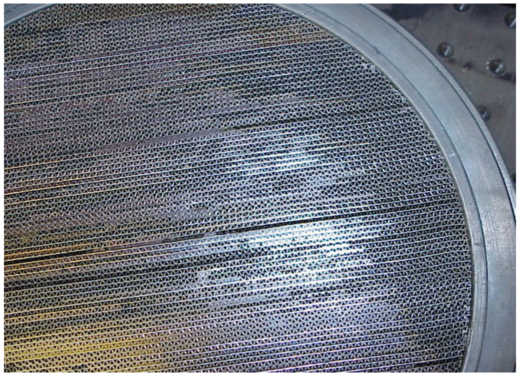

How to Improve the Tradeoff between Spatial Resolution and Sensitivity?

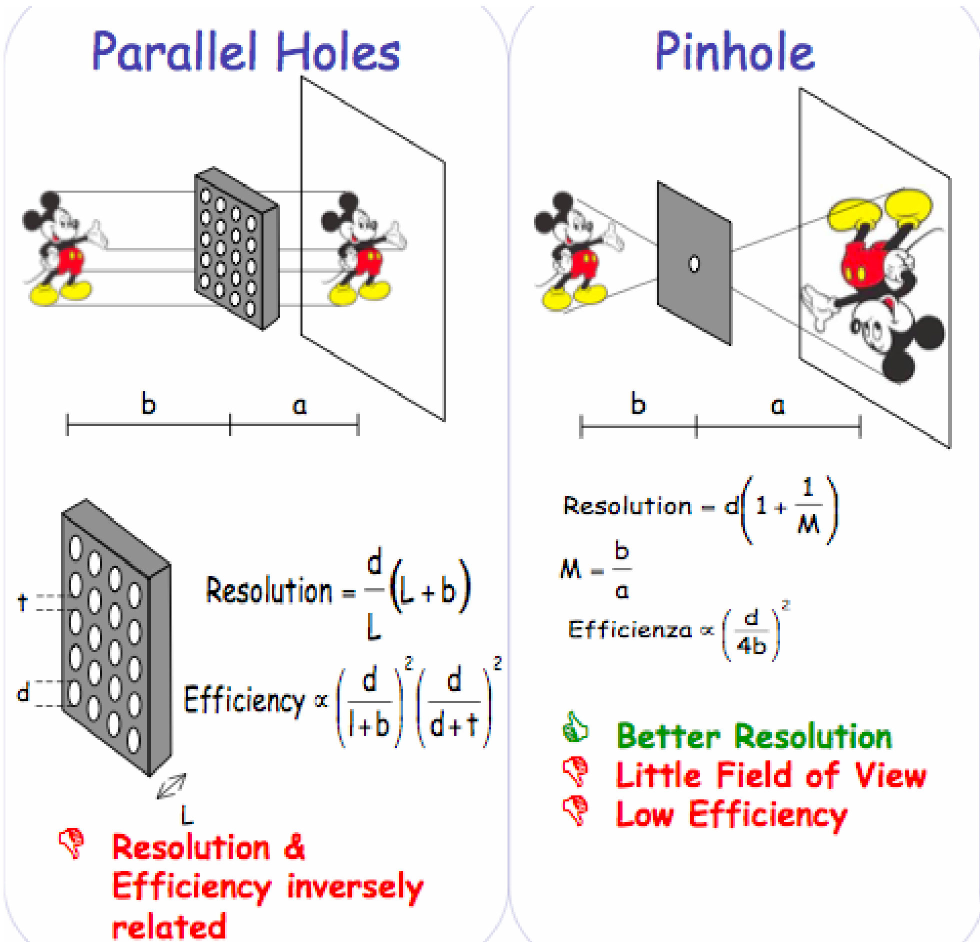

Better resolution →

- smaller hole diameter,
- better detector intrinsic resolution,
- smaller source to object distance.

Better sensitivity → Larger hole diameter

How to Improve the Tradeoff between Spatial Resolution and Sensitivity?

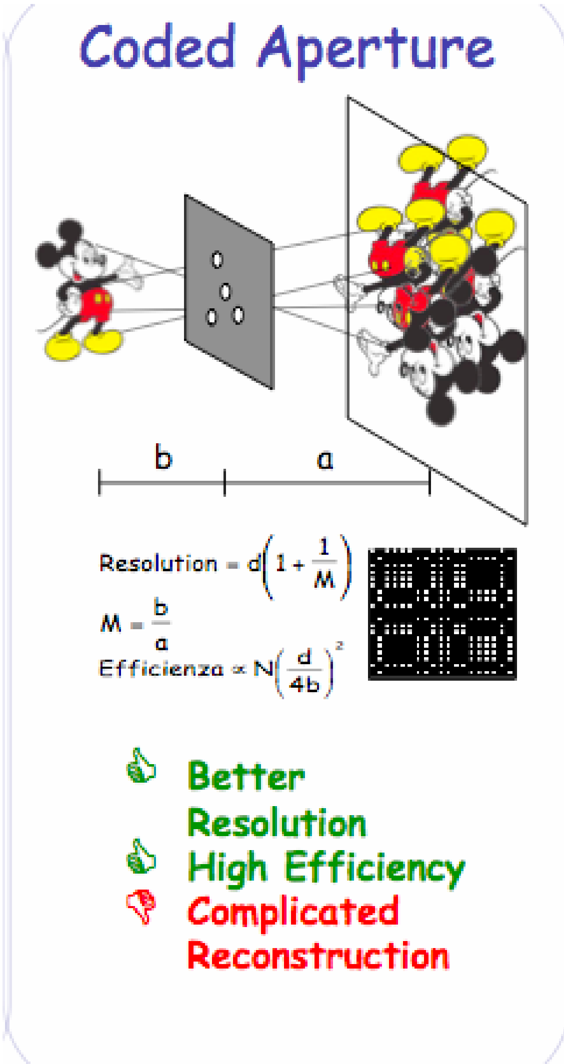

What if we increase the open fraction to allow more photons to pass through …

but split the total opening area into smaller pinholes ?

How to Improve the Tradeoff between Spatial Resolution and Sensitivity?

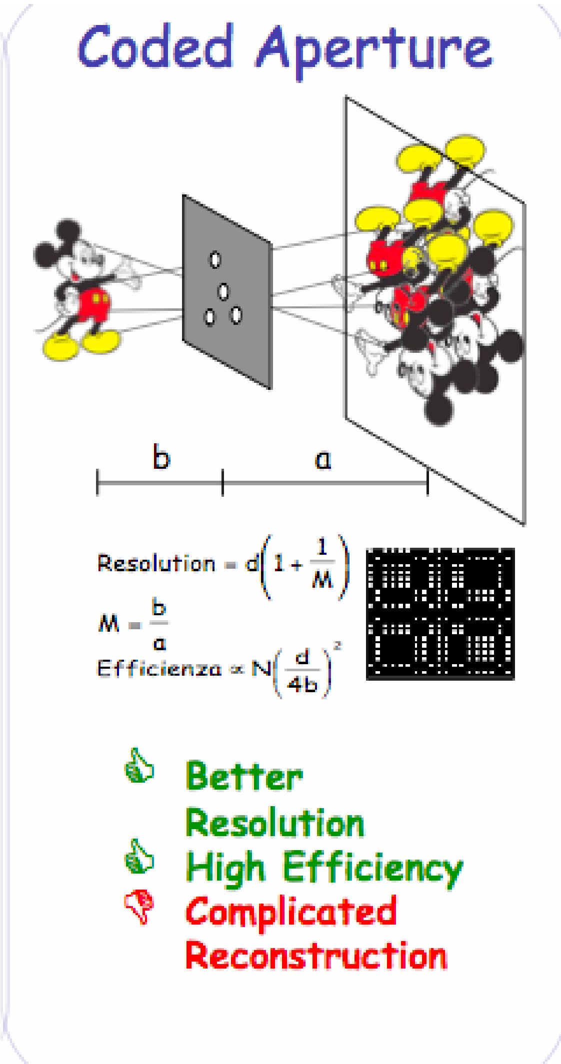

The idea of multiplexing –

- Each detected photon no longer corresponds to a unique emission location in the 2-D source plane.
- Information content per detected photon is decreased.
- No of detected photons is increased.

The Concept of Coded Aperture Imaging

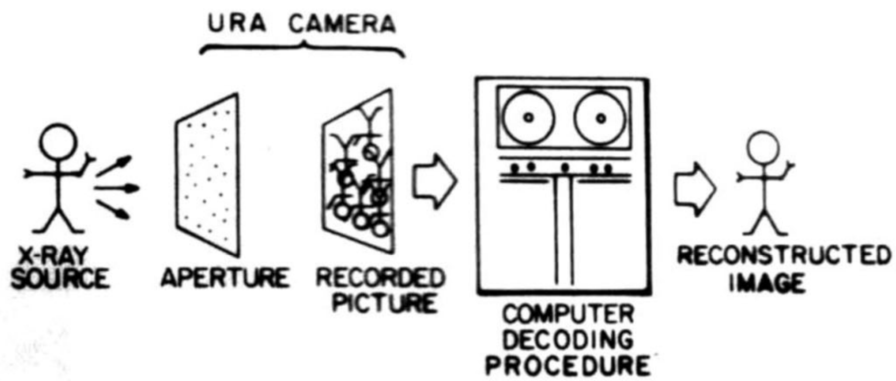

a)

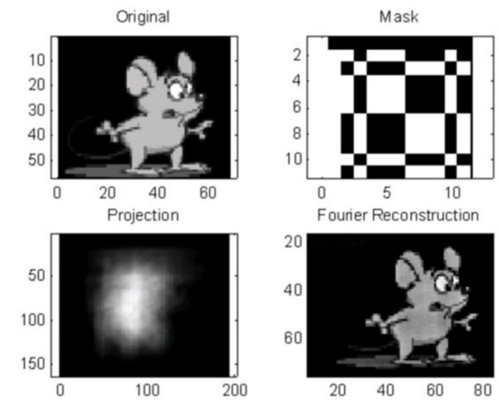

b)

Figure 1.3: a) pictorial summary of a coded aperture camera concept (here indicated with a URA camera). Adapted from [6]. b) a sample of the process from the object, through the mask, to projection and reconstruction.

For a projection A from a point source, if there are decoding partterns G that gives:

$$A \otimes G = \delta$$

Then for any projection R from an arbitary source function, the orginal source function O may be recovered by

$$\hat{O} = R \otimes G \text{ , in fact}$$

$$\hat{O} = R \otimes G = (O \times A) \otimes G = O * (A \otimes G) = O * PSF$$

Examples of Coded Apertures

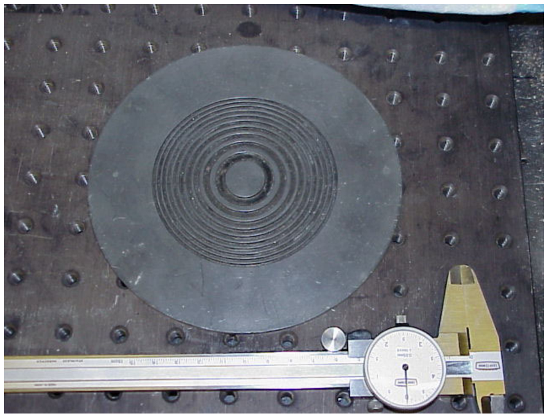

Fresnel Zone-Plate

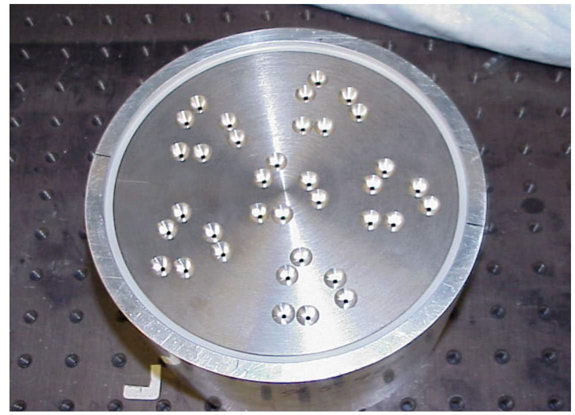

Multiple Pinhole Aperture

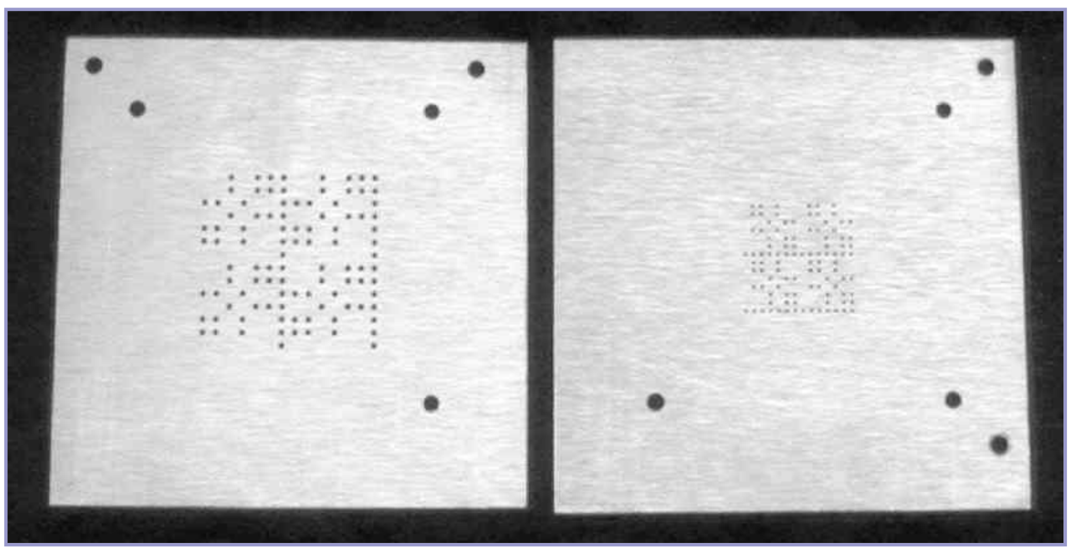

Uniformly Redundant Array Aperture, Accorsi et al, 2002

Astronomical Application of Coded Aperture Imaging

- Gamma ray source are normally point-like with very low or virtually no background.
- Sources are normally well separated between each other.
- Very low flux reaching the detector – sensitivity is very important for making quantitative conclusions.
- A wider FOV is normally required to survey a larger portion of the sky

Typical Coded Aperture Imaging System

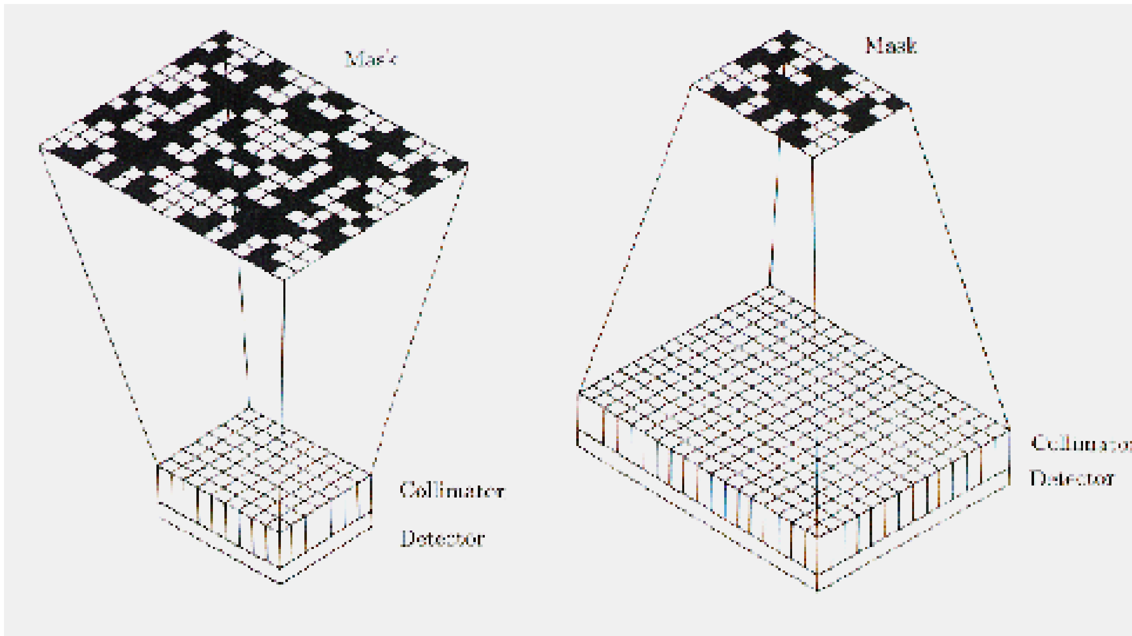

- Apertures that consists of transparent and opaque elements
- Open fraction as high as 50% (10^{-4}~10^{-3} with pinhole or parallel hole collimators.)
- Position sensitive detector used to detect the "shadow" images projecting through the mask.

Coded Aperture Imaging

Coded aperture is, from some sense, an multiple pinhole aperture with more openings ...

The way to reconstruct the image:

1. ML based method (optimum)
2. Cross-correlation – Computationally efficient, does not model detailed detector response, less optimum image quality (Please see literatures on NERS435 class website for details)

Coded aperture is the standard imaging technique in astrophysics application involving hard x-rays and gamma rays.

http://astrophysics.gsfc.nasa.gov/cai/coded_inss.html

Capabilities (as designed)

Instrument[1]/ Platform	PI/ country	Science[2]	Operat. period	Detector/ E-range (keV) E-resolution	Pattern[3] Config[4] Mask mat.	FOV[5] (degrees)/ Ang. Res. (arcmin)	Det. Area (cm^2)
Instruments flown							
(SL 602) *rocket*	A. Willmore (U. B'ham) UK	GC	69	Film 0.6-1.6	FZP Fe	110 (HM) 7.6	205
MPC *rocket*	R. Blake (U. Chicago?) USA	Sun	72	Film 0.6-1.6	ORA Ni/Fe	0.25X0.25 (HM) 0.4	2
SL 1501 *rocket*	A. Willmore (U. B'ham) UK	GC	76	PSPC 2.2-10.2 18%@6 keV	URA Fe	3.8X3.8 (ZR) 2.5X21	450
TXC *balloon*	D. Cardini (?) ?	TR	81	PSPC 10-150 20%@60 keV	URA^{1D} Pb	95X97 (ZR) 300X240	468
Burst camera / Gamma Cam *balloon*	H. Horstman (TESRE) Italy	GRB	83	NaI 30-300 20%@60 keV	ORA_{50} Pb	119 (FC) 120	1200
HXT *Tenma*	M. Tsunemi (ISAS) Japan	ASM	83-84	PSPC 2-25 20%@6 keV	URA^{1D} Fe/Cr	40X40 (HM) 60	140
DGT *balloon*	M. McConnell (UNH) USA	Crab,Cyg	84,88	BGO 160-9300 19%@662 keV	URA R|C Pb	15X23 (FC) 230	709
XRT *Spacelab 2*	A. Willmore (U. B'ham) UK	AGN, GC	85	PSPC 2-25 <20%@6 keV	URA-p R|C Fe	3.2X3.2 (HM) 3,12	1024
COMIS-TTM *Kvant-Mir*	A. Brinkman (SRON) Netherlands & UK	transients gal. ridge GC	87-99	PSPC 2-30 18%@6 keV	URA-p R|S Fe/Au	8X8 (HM) 2	655
GRIP *balloon*	T. Prince (CalTech) USA	Crab, GC	88,89, 93,95	NaI 30-10000 23%@60 keV	HURA H|C Pb/Sn	14 (HM) 66	645
(ZEBRA) *balloon*	G. Villa (TesRe) Italy	AGN, Crab, GC	89	NaI 150-10000 12%@661 keV	URA W	7X9 (FC) 60	2500
MIXE *balloon*	B. Ramsey (MSFC) USA	Crab,Cyg,AGN	89,93,97	MicroStrip 25-100 6%@60 keV	URA R|C W	1.8X1.8 (HM) 6.9	784
SIGMA *Granat*	J. Paul (CNES) France	GC, XB	89-99	NaI 30-1500 16%@60 keV	URA-h R|C W	11X11 (HM) 13	5000
ART-P *Granat*	R. Sunyaev (IKI) Russia	GC	89-93	PSPC 2-30 22%@6 keV	URA-h R|S Cu	1.8X1.8 (HM) 6	655
(Gamma-1) *Gamma*	V. Akimov? (IKI) SU	GC, Sun	90-92	Spark 35-1300 16%@60 keV	URA^{1D} W	24 (HM) 20	1500
(URA) *STS 39*	E. Fenimore (LANL) USA	GC, Cen X-3	91	HP-GSPC 2-70 15%@6 keV	URA H|C W	4.5 (HM) 4	1000
EXITE-2 *balloon*	J. Grindlay (Harvard) USA	GC	93	NaI 20-600 18%@60 keV	URA R|C Pb/Sn/Cu	4.7X4.7 (HM) 23	1600
TIMAX *balloon*	J. Braga (INPE) Brazil	GC	93	NaI 30-100 25%@60 keV	URA R|M/A Pb/Cu	12X8.5 (ZR) 120	400
SAGE *balloon*	G. Skinner (U B'ham) UK	Crab	93	Ge 20-1500 <0.5%	ORA Pb	16X4 (FC) 60	20

And many more …

An Typical Emission Tomography System Described in Matrix Form

The response function of the imaging system for an impulse signal at a given source location – The Impulse Response Function h_i

$$
\begin{pmatrix} g_1 \\ g_2 \\ g_3 \\ \vdots \\ g_M \end{pmatrix} = \begin{pmatrix} p_{11} & p_{12} & p_{13} & \cdots & p_{1N} \\ p_{21} & p_{22} & p_{23} & \cdots & p_{2N} \\ p_{31} & p_{32} & p_{33} & \cdots & p_{3N} \\ \vdots & \vdots & \vdots & \ddots & \vdots \\ p_{M1} & p_{M2} & p_{M3} & \cdots & p_{MN} \end{pmatrix} \begin{pmatrix} f_1 \\ f_2 \\ f_3 \\ \vdots \\ f_N \end{pmatrix}
$$

No. of counts observed on a given detector pixel

p_{mn}: the probability of a gamma ray generated at source pixel m being detected by detector pixel n.

f_n: No. of gamma rays generated in a given source pixel

Image Formation with Coded Apertures

Once the overlapping projection data is acquired, the underlying image of the source object can be recovered using the many reconstruction techniques, such as the ML based iterative approach

So the ML reconstruction for Poisson distributed data is

$$\hat{\boldsymbol{f}}_{\boldsymbol{ML}} = \arg\max_{\boldsymbol{f}} l(\boldsymbol{f},\boldsymbol{g}) = \arg\max_{\boldsymbol{f}} \left[\sum_{m=1}^{M} \left(g_m \log \bar{g}_m - \bar{g}_m - \log g_m! \right) \right]$$

since g_m is not function of $\boldsymbol{f}$, we get

$$\boxed{\hat{\boldsymbol{f}}_{\boldsymbol{ML}} = \arg\max_{\boldsymbol{f}} l(\boldsymbol{f},\boldsymbol{g}) = \arg\max_{\boldsymbol{f}} \left[\sum_{m=1}^{M} \left(g_m \log \bar{g}_m - \bar{g}_m \right) \right]}$$

Electronic Collimation
Compton Camera

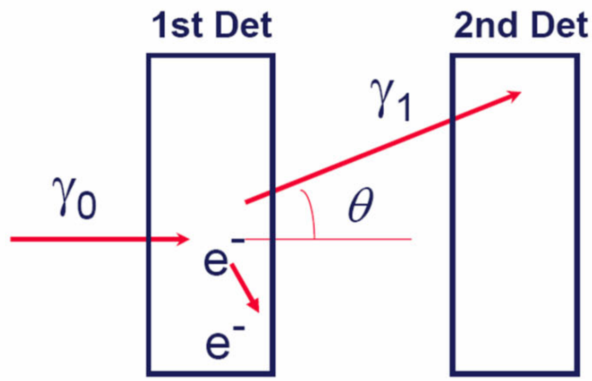

$$\frac{1}{E_1} - \frac{1}{E_0} = \frac{1}{511\text{keV}}(1-\cos\theta)$$

E_0: incident photon energy
E_1: scattered photon energy
θ : scattering angle

1st det: solid state detector
2nd det: scintillation detector

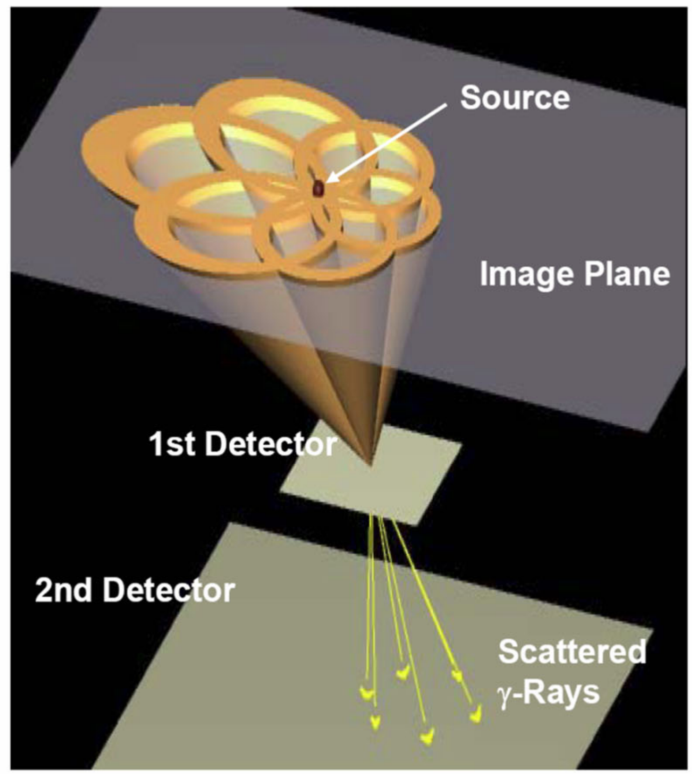

Courtesy of Neal Clinthorne, U. Michigan.

Energy Transfer in Compton Scattering

If we assuming the electron is free and at rest, the scattered gamma ray has an energy

Initial photon energy, v: photon frequency,

h= 6.757704 meter ·kilogram/second, (Planck’s constant)

$$hv' = \frac{hv}{1 + \frac{hv}{m_0 c^2}(1 - \cos(\theta))},$$

mass of electron

Scattering angle

and the photon transfers part of its energy to the electron (assumed to be at rest), which is known as a recoil electron. Its energy is simply

$$E_{recoil} = hv - hv' = hv - \frac{hv}{1 + \frac{hv}{m_0 c^2}(1 - \cos(\theta))}$$

The one-to-one relationship between scattering angle and energy loss!!

Reading: Page 51, Radiation Detection and Measurements, Third Edition, G. F. Knoll, John Wiley & Sons, 1999.

Derivation of the Relation Between Scattering Angle and Energy Loss

The relation between energy the scattering angle and energy transfer can be derived based on the conservation of energy and momentum:

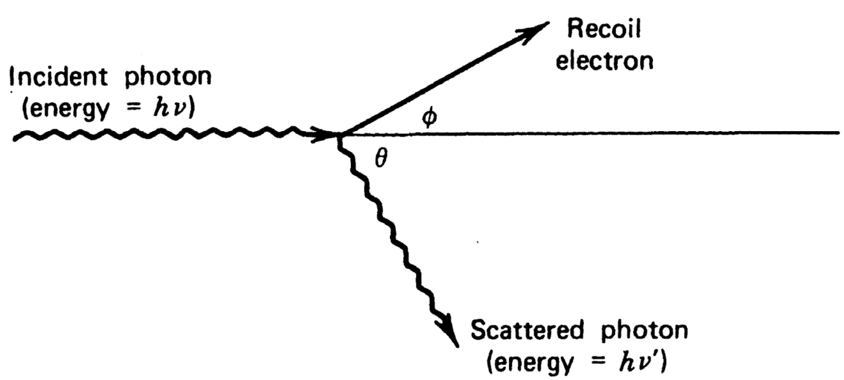

$$\breve{p}_{hv} + \breve{p}_{e} = \breve{p}_{hv'} + \breve{p}_{e'}$$

$$E_{hv} + E_{e} = E_{hv'} + E_{e'}$$

Are those terms truly zero?

Compton Scattering with Non-stationary Electrons – Doppler Broadening

Comparison of the photon spectra scattered by C and Cu samples. E_{hv}=40keV, θ=90 degrees

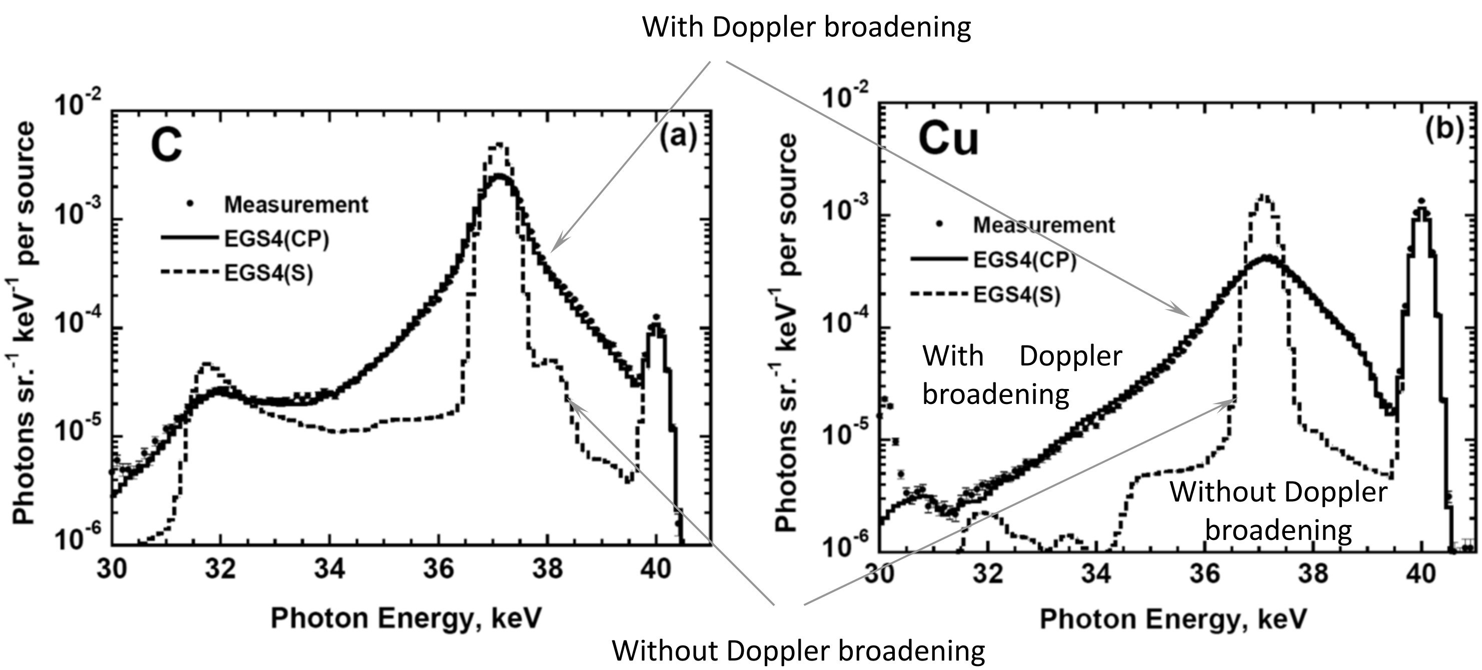

The Doppler broadening is stronger in Cu than in C because Cu electrons have greater bonding energies.

Electronic Collimation

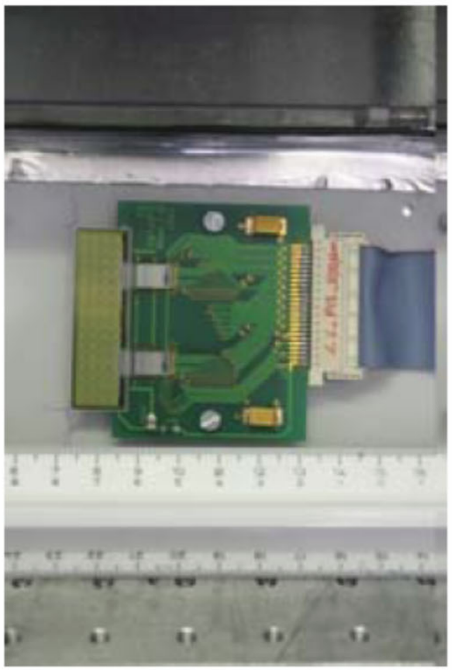

Silicon pad first detector

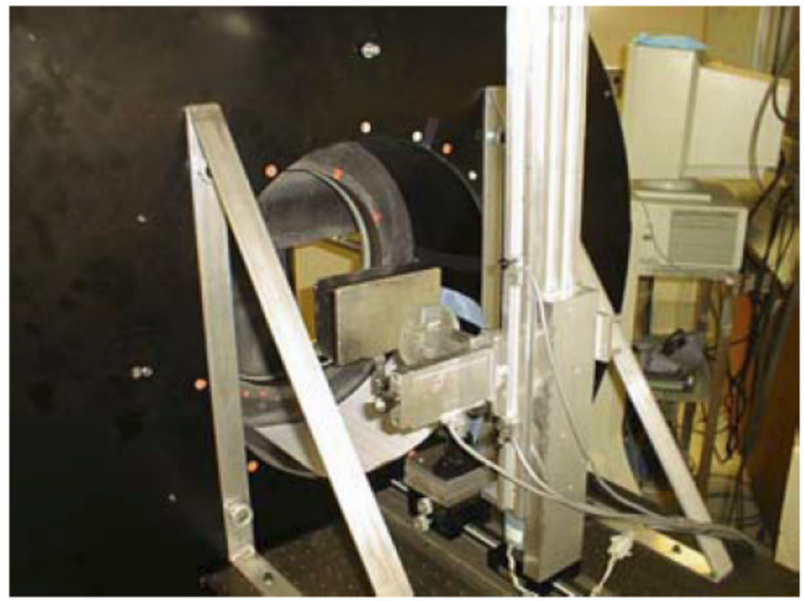

Compton camera

Courtesy of Neal Clinthorne, U. Michigan.

Electronic Collimation

Advantages

- ***Spatial resolution and efficiency are more decoupled than with absorbing collimation – very high efficiency***
- ***Performance improves dramatically with increasing energy – high resolution***

Challenges

- ***Very low noise required for first detector (~1 keV or less at 140 keV)***
- ***System is electronically complex***
- ***Image reconstruction is computationally challenging***

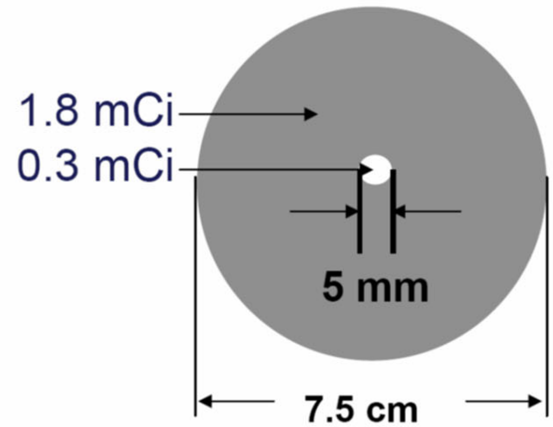

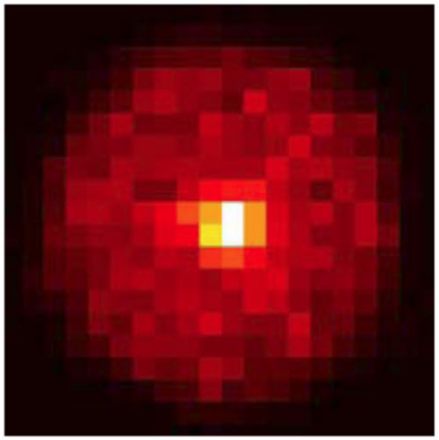

Reconstruction of I-131 phantom

Courtesy of Neal Clinthorne, U. Michigan.

The Comptel Observatory

- Compton telescopes are two-level instruments.
- Typically sensitive to photons between 300 eV and 30 MeV.
- Top level = photon Compton scatters in liquid scintillator.
- Bottom level = Scattered photon travels down and is absorbed by crystal scintillator.
- PMTs triggered on both levels.

Courtesy of Neal Clinthorne, U. Michig

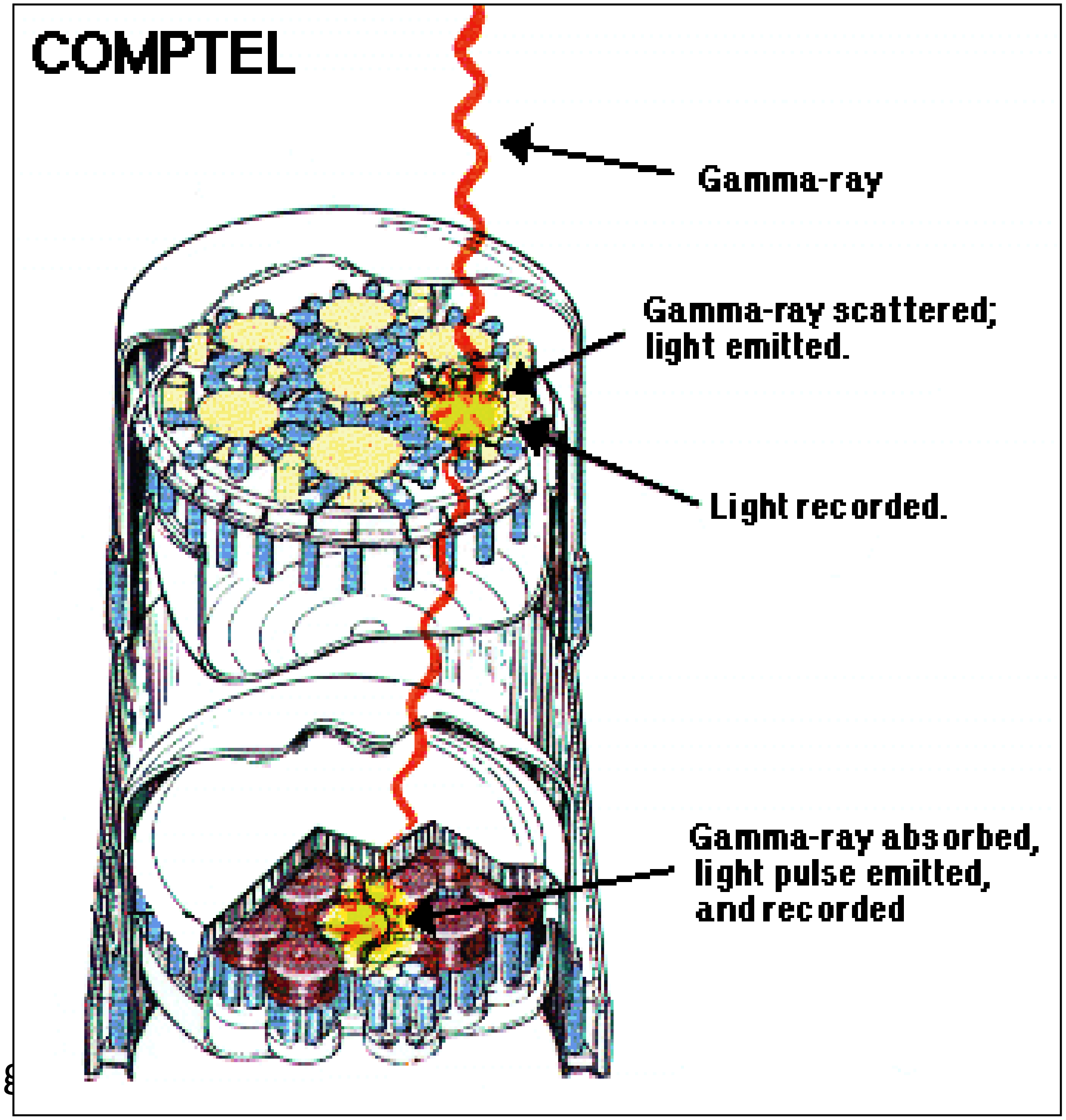

The Comptel Observatory

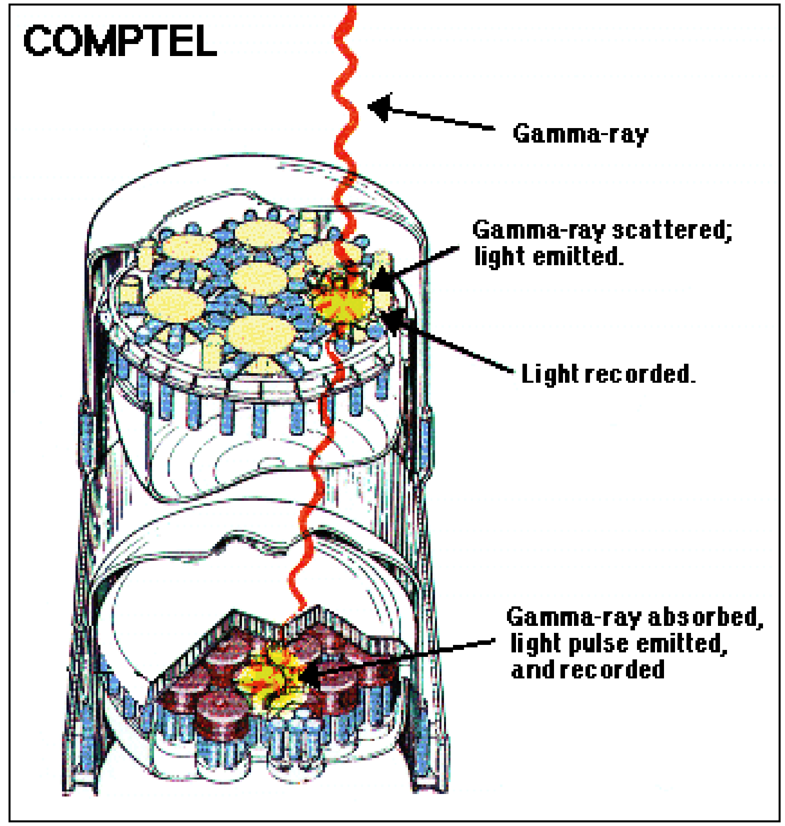

The Compton Gamma Ray Observatory was the second of NASA's Great Observatories. Compton, at 17 tons, was the heaviest astrophysical payload ever flown at the time of its launch on April 5, 1991 aboard the space shuttle Atlantis. Compton was safely deorbited and re-entered the Earth's atmosphere on June 4, 2000.

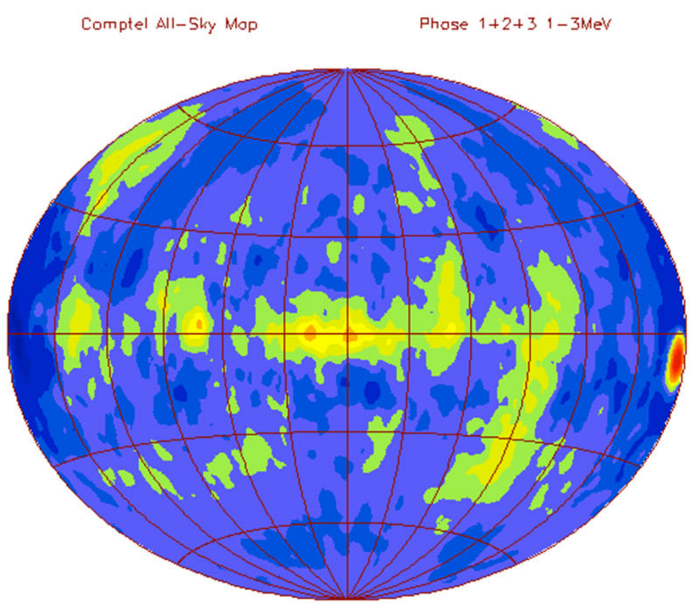

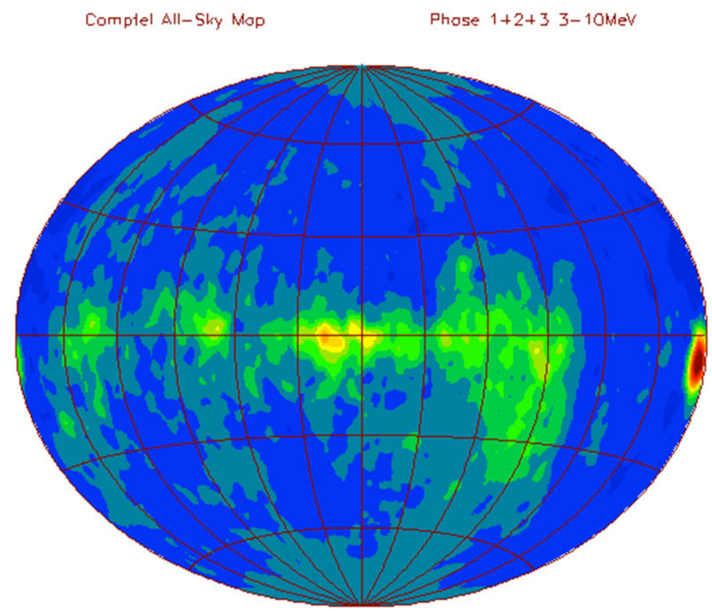

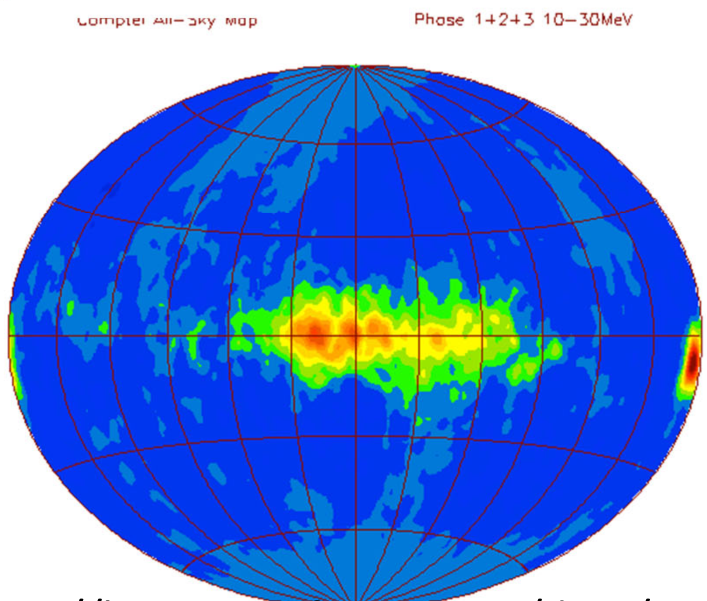

http://heasarc.gsfc.nasa.gov/docs/cgro/comptel/allsky.html

Grazing Incidence Telescope

Uses fact that x-rays and gamma rays at very short wavelengths behave like ordinary light rays if they strike surfaces at a shallow enough angle.

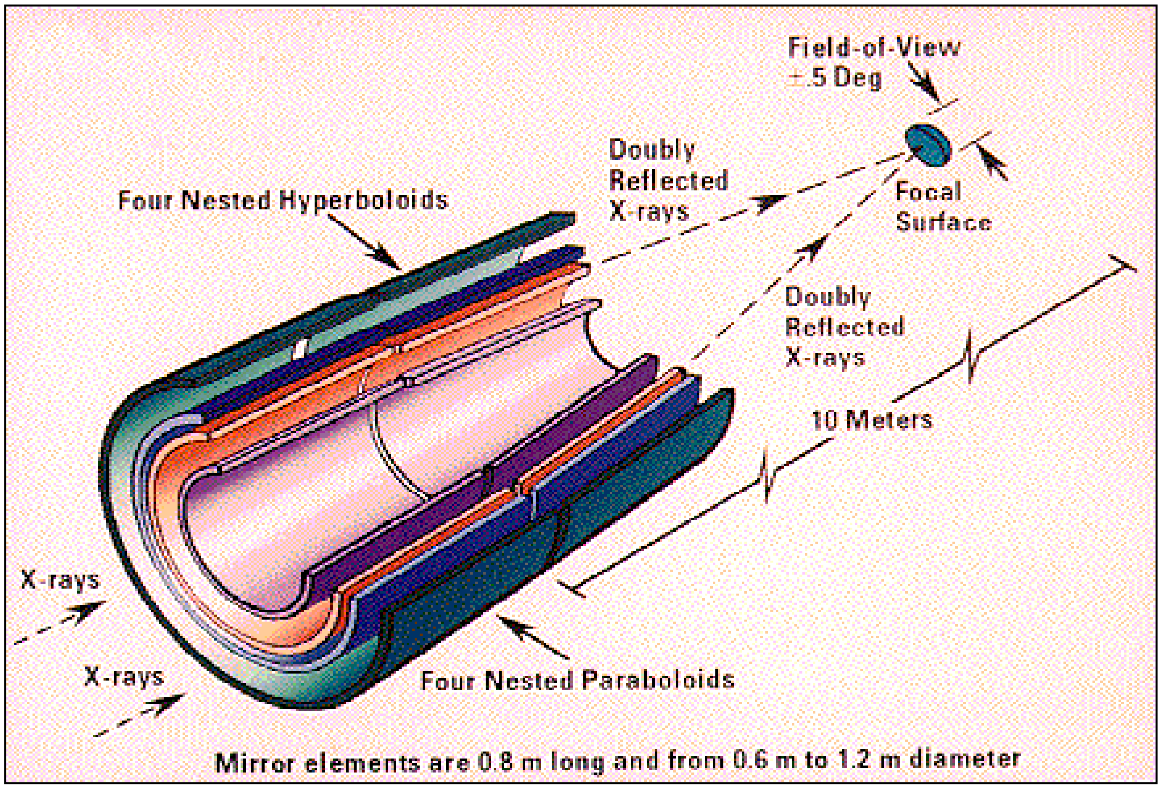

Only work if angle of reflection is very low (typically 10 arc-minutes to 2 degrees).

The Chandra X-ray Observatory

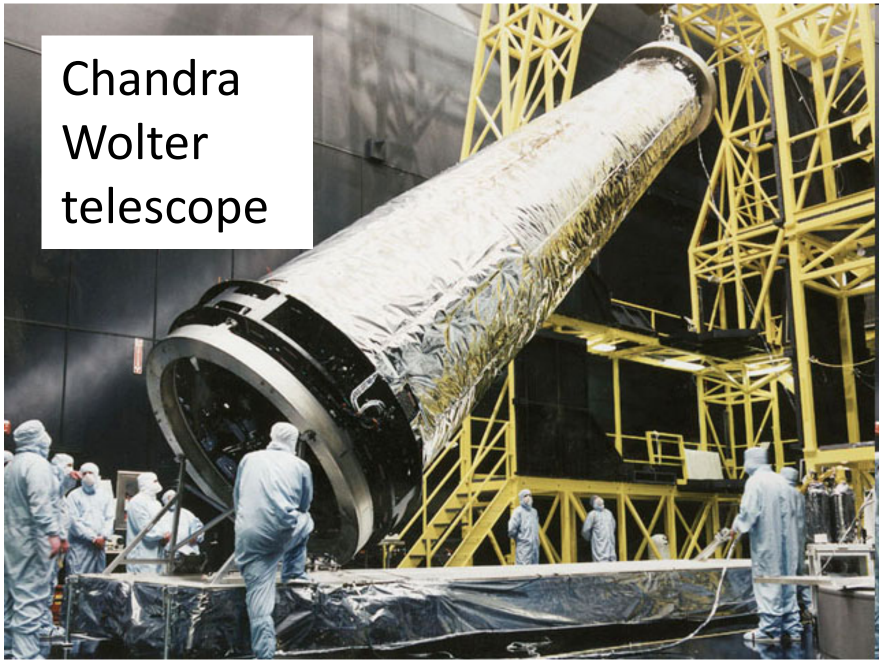

The ROSAT X-ray Observatory

ROSAT (1990-1999) the ROentgen SATellite, was an X-ray observatory designed to make an all-sky survey in soft x-rays (0.1 keV-2 keV). Its sensitivity to X-rays was over 1000 times greater than Uhuru. The X-ray mirror assembly was a grazing incidence four-fold nested Wolter I telescope with an 84 cm diameter aperture.

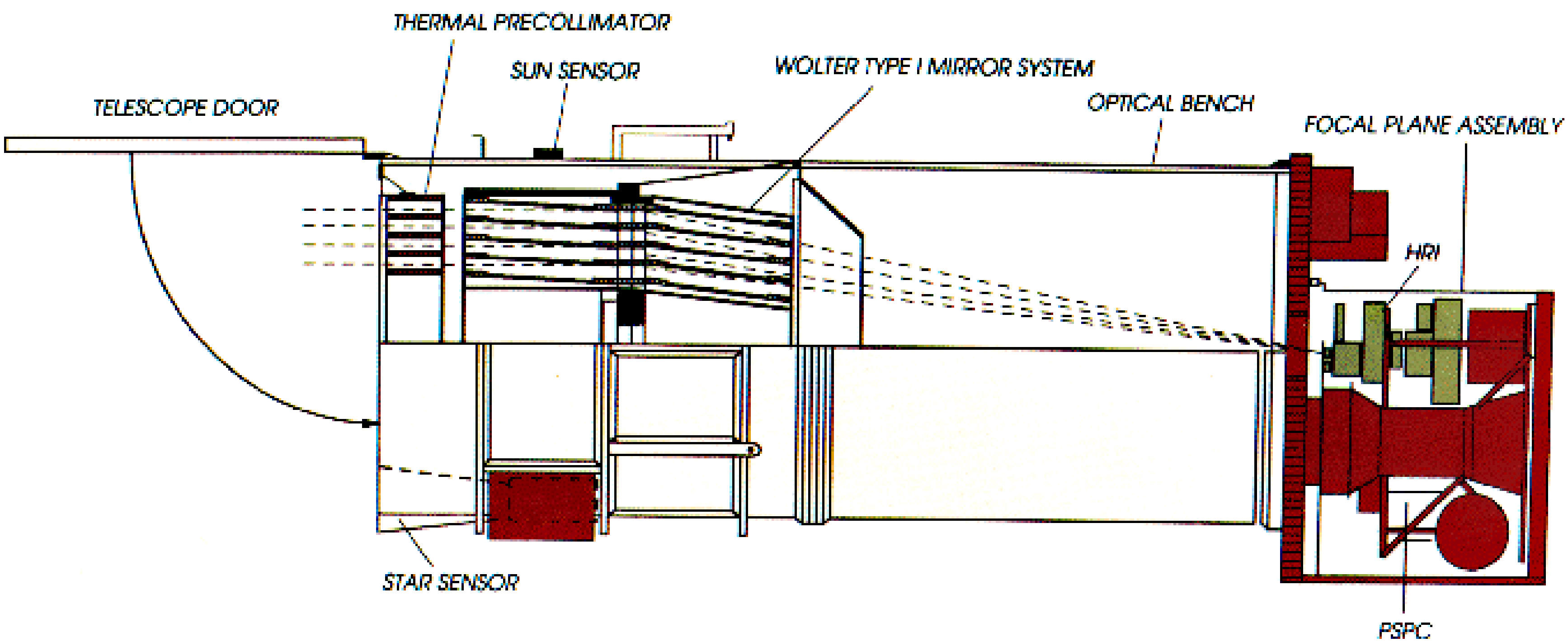

Electronic Collimation

Why electronic collimation?

Each detector element is allowed to see greater source volume
→ high sensitivity

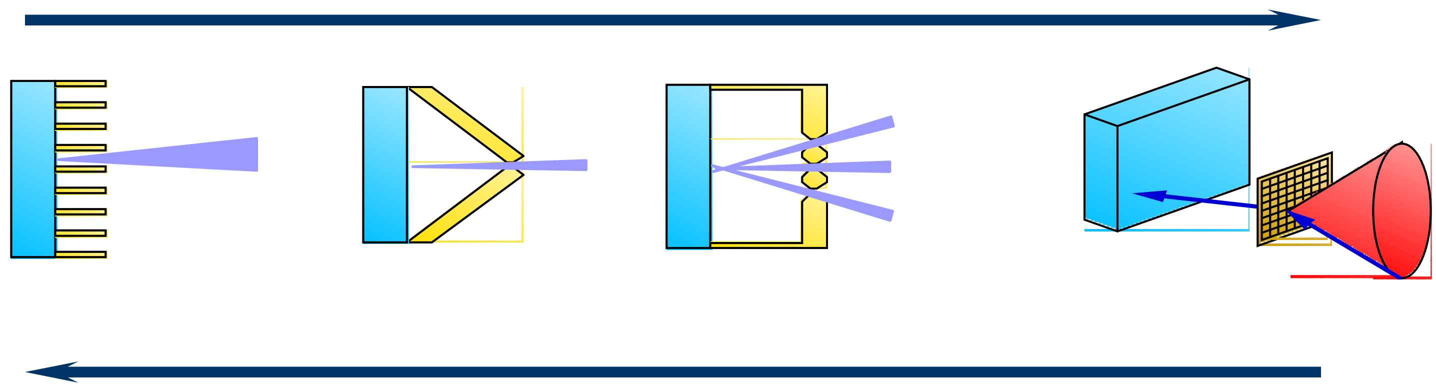

Information content per detected photon is decreasing → the benefit depends on the particular source.

Single Photon Emission Computed Tomography

SPECT

Each projection view is 2-Dimensional → true 3-Dimensional imaging technique (cf. X-ray CT)

Spatial resolution of 10~15mm with 1 rotating camera

Clinical applications :

- Detection of tumor
- Assessing myocardial infarction
- Blood perfusion in the brain

Typical imaging time : ~30min with 1 camera

Recent advances: new detector systems, improving the trade-off between spatial resolution & detection efficiency, new radio-labeled pharmaceuticals

Detection Systems

Modern Clinical Systems

GE Millenium VG

Philips Cardio 60

Siemens e.cam
Variable Angle

Detection Systems

Requirements:

- Good energy resolution for Compton scattering rejection
- High detection efficiency for radionuclides of interest
- Sufficient spatial resolution so that it does not limit overall system resolution
- Low dead-time at count rates of interest

Conventional Anger Camera

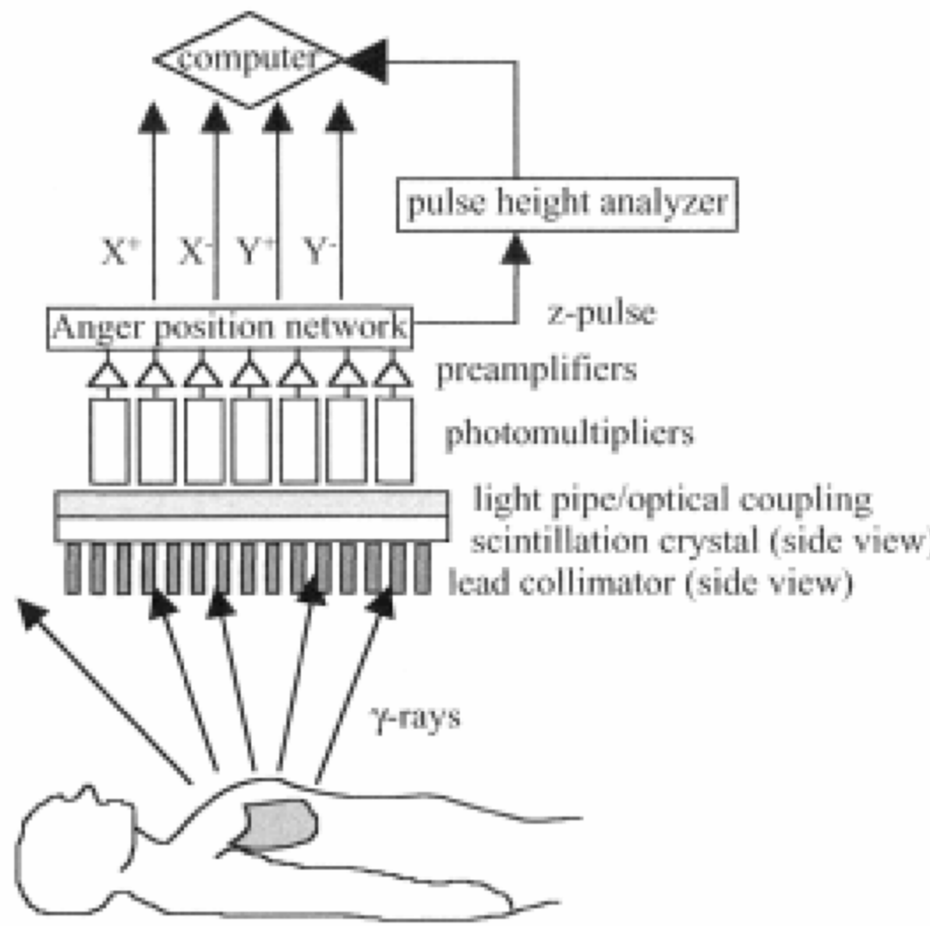

FIGURE 2.4. Schematic diagram of a gamma camera positioned above the patient. The distribution of the radiopharmaceutical is indicated by the shaded region within the body.

Conventional Anger Camera

- PMTs coupled to large, continuous NaI(Tl) crystal
- Spatial resolution 3–4 mm FWHM
- Energy resolution 8–10% FWHM
- Mature technology (DoB ~1957)
- Large-area, >40cm x 40cm typical
- Simple and cost-effective

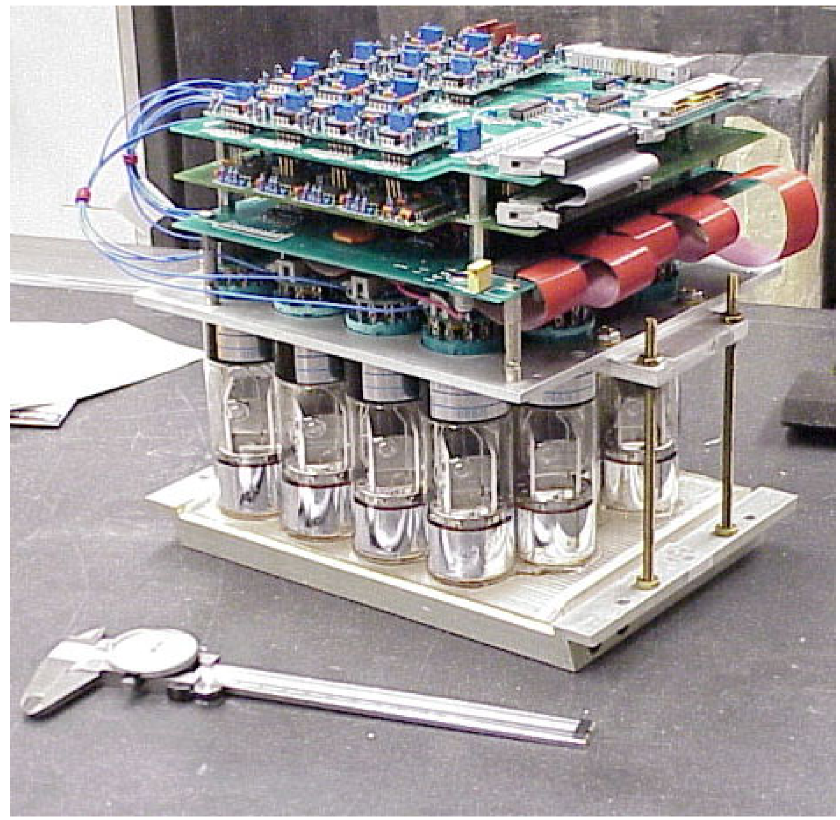

SPRINT II camera module

Scintillation Crystal Used in Gamma Cameras

- Crystal (typically NaI) scintillates with blue light in a linear fashion related to gamma ray energy.
  - Grown crystal
  - Hydroscopic (H_2O sensitive)

- Thickness used depends upon energy measured. Thickness goes up as energy increases

- 13% of gamma energy -> light

- New detector technology uses solid state crystals – Cadmium Zinc Telluride (CZT)

Scintillation Crystal Properties

TABLE 1 Properties of Common Scintillation Crystals Used in Small-FOV Imager Designs

Scintillator	Effective Z	Density (g/cc)	Radiation Length (mm)[a]	Relative Light Yield	Refractive Index	Decay Time (ns)	Peak Emission Wavelength (nm)	Hygroscopic?	Rugged?
NaI(Tl)	51	3.67	3.4	100	1.85	230	410	Yes	No
CsI(Tl)	54	4.51	2.2	135	1.79	1000	530	No	Yes
CsI(Na)	54	4.51	2.2	75	1.79	650	420	No	Yes
BGO	74.2	7.13	10.5	15	2.15	300	480	No	Yes
LSO(Ce)	65.5	7.4	11.6	75	1.82	40	420	No	Yes
CaF_2(Eu)[b]	16.9	3.17	N/A	50	1.43	940	435	No	Yes

[a]Radiation lengths for NaI(Tl), CsI(Tl) and CsI(Na) are for 140-keV photons; Values for BGO and LSO are at 511 keV.
[b]CaF_2(Eu) is used in beta imaging.

Detection efficiency

No. of visible photons per interaction

Efficiency for converting the light signal to electronic signal

Scintillation Light

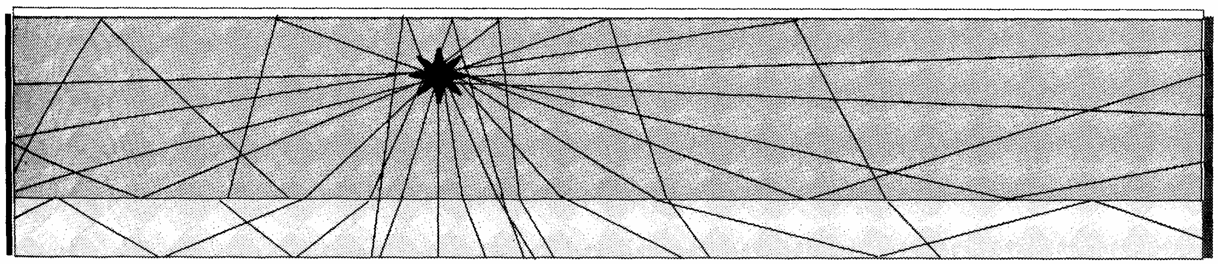

FIGURE 4 Representation of light ray propagation from a point source of light within a scintillation crystal slab with a white diffuse Lambertian reflector on top, absorbing sides, and a light diffuser on the bottom leading into the photodetector.

- Scintillation light are generated isotropically.
- It is difficult to control light propagation inside a continuous bulk scintillator
- Light spreading leads to loss in both spatial resolution and energy resolution.
- Normally, the best we can do is to provide a better boundary condition for a better light collection efficiency.

Scintillation Photons Emitting from the Crystal

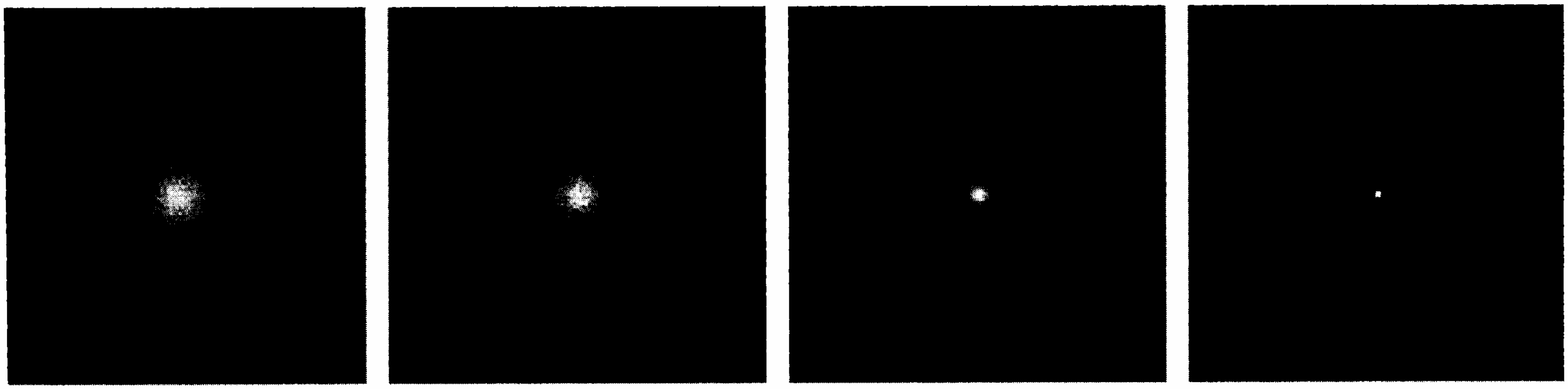

FIGURE 5 Light distribution seen at bottom of a $6 \times 6 \times 0.6\ cm^3$ NaI(Tl) crystal for four depths from the top of the crystal of a point light source. The light spread widths are 9.2, 7.2, 3.5, and 0.7 mm FWHM, respectively.

light distribution shared over multiple photodetector elements with an Anger-type positioning scheme is governed by Poisson statistics (Tanaka *et al.*, 1970; Barrett and Swindell, 1981):

$$R_{\lim} = 2.35\left(\sum_i \frac{(dn_i / dx)^2}{n_i}\right)^{-1/2} \qquad (4)$$

An optional observation:

n_i is the number of photons at the ith spatial location. Suppose we know the distribution of the light pool, so we can derive how the no. of photons changing with spatial location x.

Continuous and Discrete Crystals

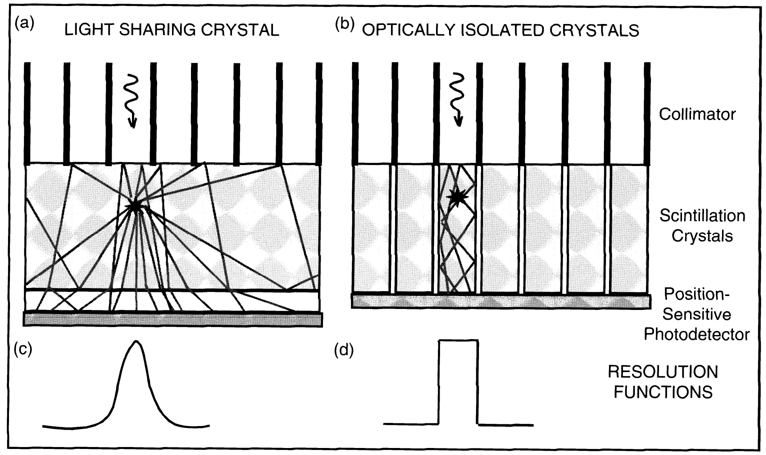

FIGURE 6 Schematic drawings of the light ray propagation for typical (a) single and (b) multiple scintillation crystal camera designs. For the pixellated design, scintillation light is confined to one crystal and focused on one spot of the photodetecting array. (c,d) Approximate shapes of the resulting theoretical intrinsic point spread functions for single-photon imaging.

Continuous:

- Photons reaching detector surface after a few reflection or refraction – better light collection efficiency.
- Light spread is wide → (a) poor resolution (b) suffers from detector non-uniformity.

Discrete:

- Multiple reflection before collection.
- Light collection is degraded → depending on interaction depth.
- Internal (total) reflection is the best way to key the photon inside.

The Light Transport in Discrete Crystals

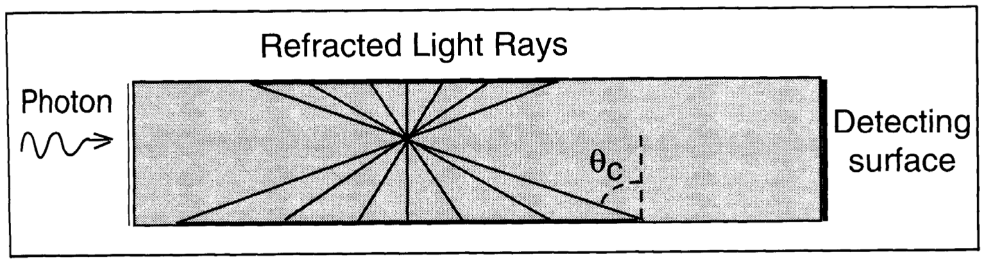

FIGURE 7 Depiction of the fraction of scintillation light lost from refraction through the sides of a long and narrow scintillation crystal for all incident angles less than the critical angle, θ_c. High-energy photons enter the crystal from the left and only a fraction of the scintillation light created is piped down to the detecting surface at the right.

- Air gap is maintained around the side walls of each elements.
- Crystals with larger refraction index provide better light collection.

The Photomultiplier Tube

Photomultiplier Tube (PMT)

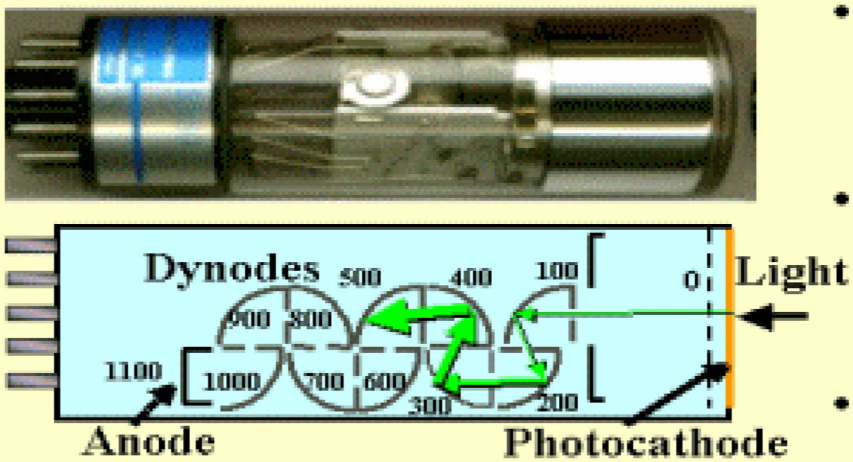

- Converts visible light (scintillation) into an electronic pulse
- Electron amplification through a series of dynodes
- Overall gain ~ 10^6

Light hitting the photocathode liberates electrons which are accelerated through a series of dynodes. The electron gain at each dynode is ~ 4.

The Photomultiplier Tube

Other electron multiplication structures

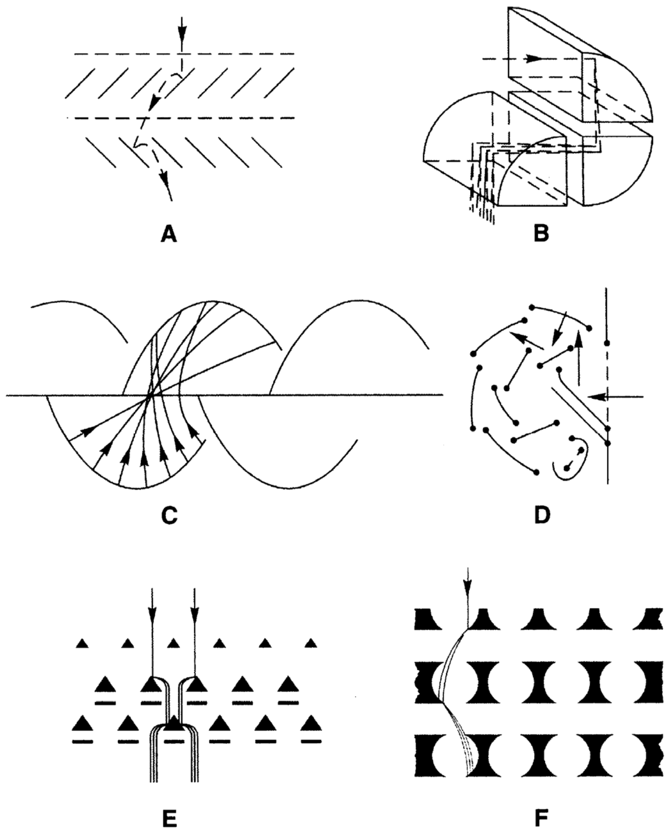

FIGURE 2 Scheme of dynode configurations: (a) venetian blind dynodes, (b) box dynode structure, (c) linear focusing dynodes, (d) circular cage dynodes, (e) mesh dynodes, and (f) foil dynodes. (From Photonis, 1994, *Photomultiplier Tubes: Principles and Applications*.)

Typical power supply unit

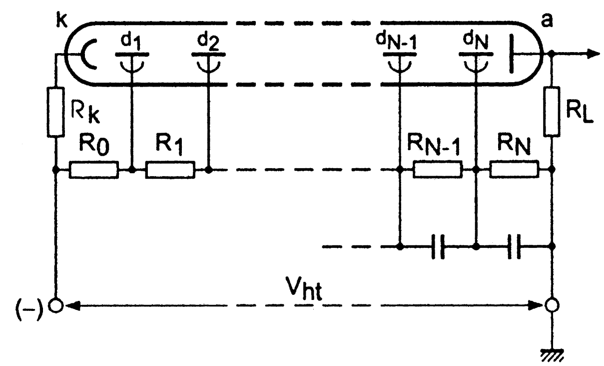

FIGURE 4 High-voltage PMT resistor network with the anode grounded and the cathode at negative high-voltage polarity. (From Photonis, 1994, *Photomultiplier Tubes: Principles and Applications*.)

- PMTs has gone through many generations.
- They are simple, robust and in many cases reasonably cost-effective.

The down side:

- Relatively low quantum efficiency → only 1 in 5 incident photons are converted to photonelectron.

Position Sensitive Photomultiploer Tubes

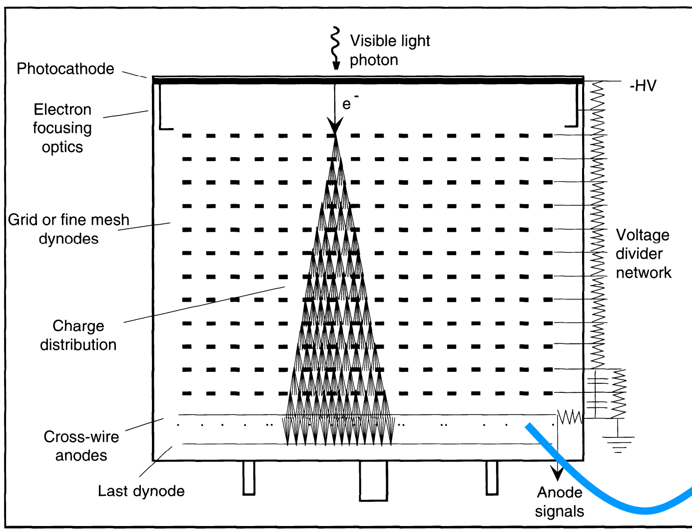

FIGURE 11 Depiction of the cross-wire anode PSPMT and its signal formation process. For simplicity, the charge avalanche created from only a single photoelectron is shown. A 10^5 photoelectron amplification factor is typical. Setting the cathode at ground and biasing the anode at +HV through a coupling capacitor is also possible.

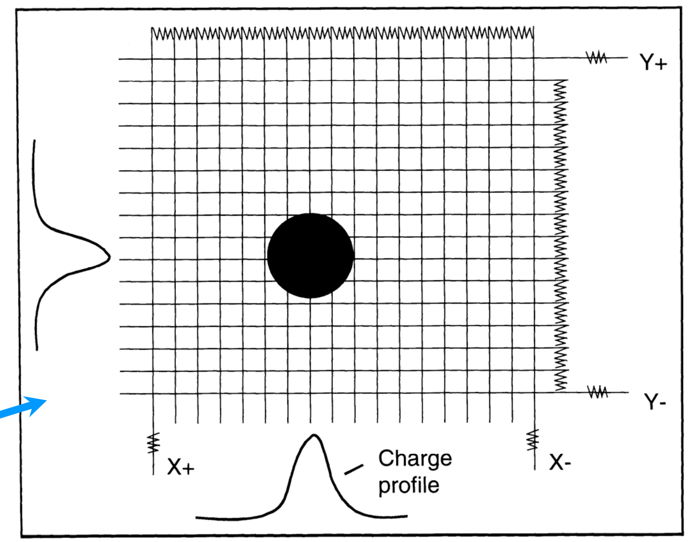

FIGURE 13 Example depiction of resistive charge division readout scheme for event positioning with a cross-wire anode PSPMT.

The cross-wire readout circuitry

PSPMT + Pixellated Scintillator

Advantages

- Small size useful for niche applications
- Pixellated scintillator → high spatial resolution

Disadvantages

- Quantum efficiency (~25%)
- Pixelated scintillator has poorer energy resolution (>10%) than continuous
- Small size is inadequate for many applications (human SPECT)
- Expensive!

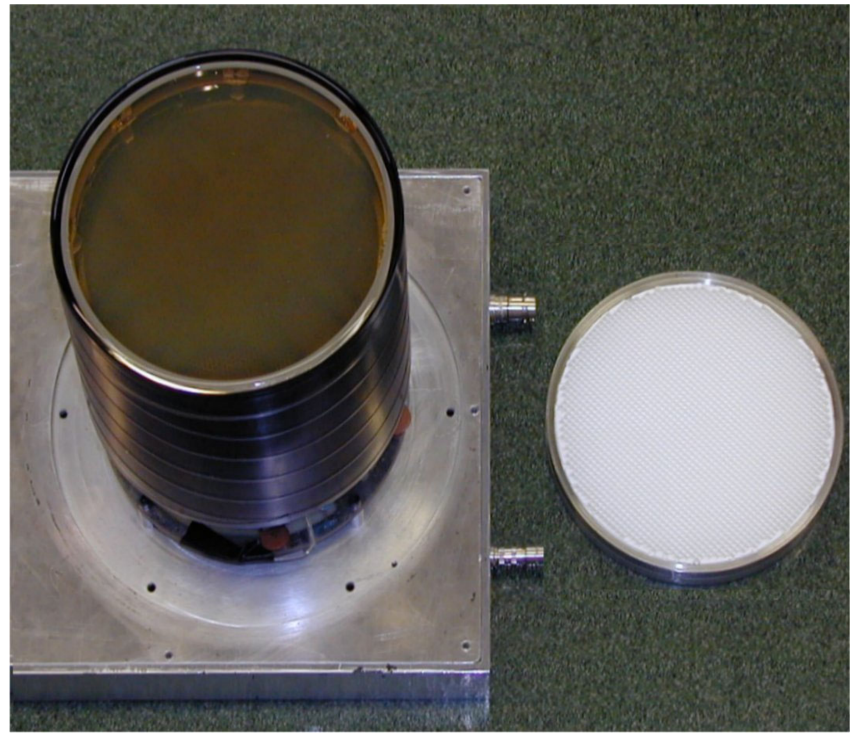

Scintillation Crystal Properties

TABLE 1 Properties of Common Scintillation Crystals Used in Small-FOV Imager Designs

Scintillator	Effective Z	Density (g/cc)	Radiation Length (mm)[a]	Relative Light Yield	Refractive Index	Decay Time (ns)	Peak Emission Wavelength (nm)	Hygroscopic?	Rugged?
NaI(Tl)	51	3.67	3.4	35,000/MeV 100	1.85	230	410	Yes	No
CsI(Tl)	54	4.51	2.2	135	1.79	1000	530	No	Yes
CsI(Na)	54	4.51	2.2	75	1.79	650	420	No	Yes
BGO	74.2	7.13	10.5	15	2.15	300	480	No	Yes
LSO(Ce)	65.5	7.4	11.6	75	1.82	40	420	No	Yes
$CaF_2(Eu)$[b]	16.9	3.17	N/A	50	1.43	940	435	No	Yes

[a]Radiation lengths for NaI(Tl), CsI(Tl) and CsI(Na) are for 140-keV photons; Values for BGO and LSO are at 511 keV.
[b]$CaF_2(Eu)$ is used in beta imaging.

Consider

- 100keV produces 3500 photons
- 40% light collection
- 20% quantum efficiency (photoelectron/photon)

Total signal generated on the PMT:

280 photoelectrons

Modern Readout Electronics for Scintillation Cameras

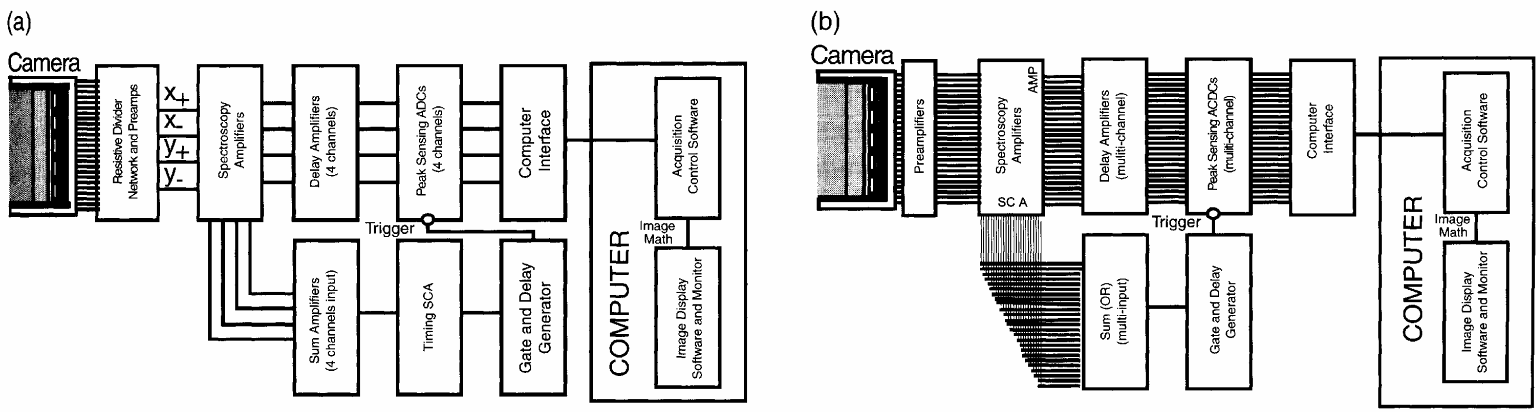

FIGURE 14 Basic examples of electronic processing topologies for image acquisition for the (a) resistive charge division readout and (b) parallel readout schemes.

Two flavors: charge sharing scheme and fully discrete readout methods

Further Broadening in Energy Spectrum

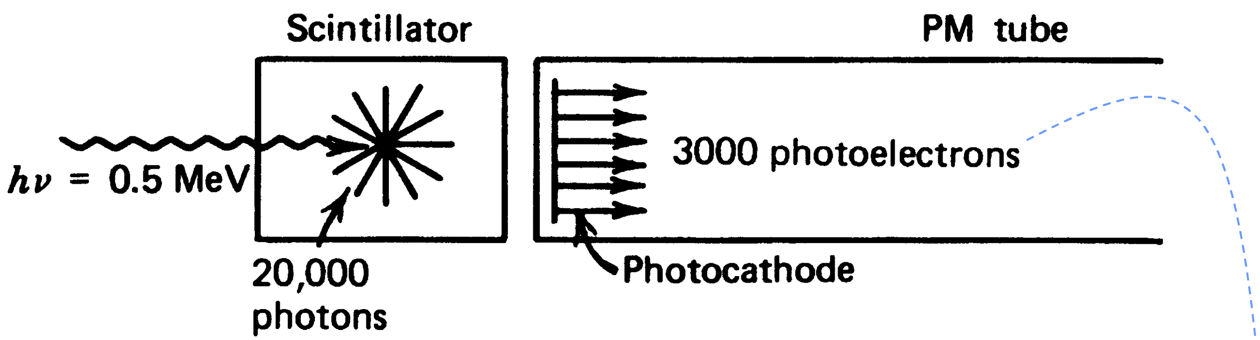

The number of photoelectrons → a Poisson variable

Energy resolution due to Poisson fluctuation on the number of photoelectrons

$$R \equiv \frac{\text{FWHM}}{H_0} = K\frac{\sqrt{E}}{E} = \frac{K}{\sqrt{E}}$$

where K is a constant of proportionality. The energy resolution should thus be inversely proportional to the square root of the gamma-ray energy.

Camera Energy Spectrum at 140 keV

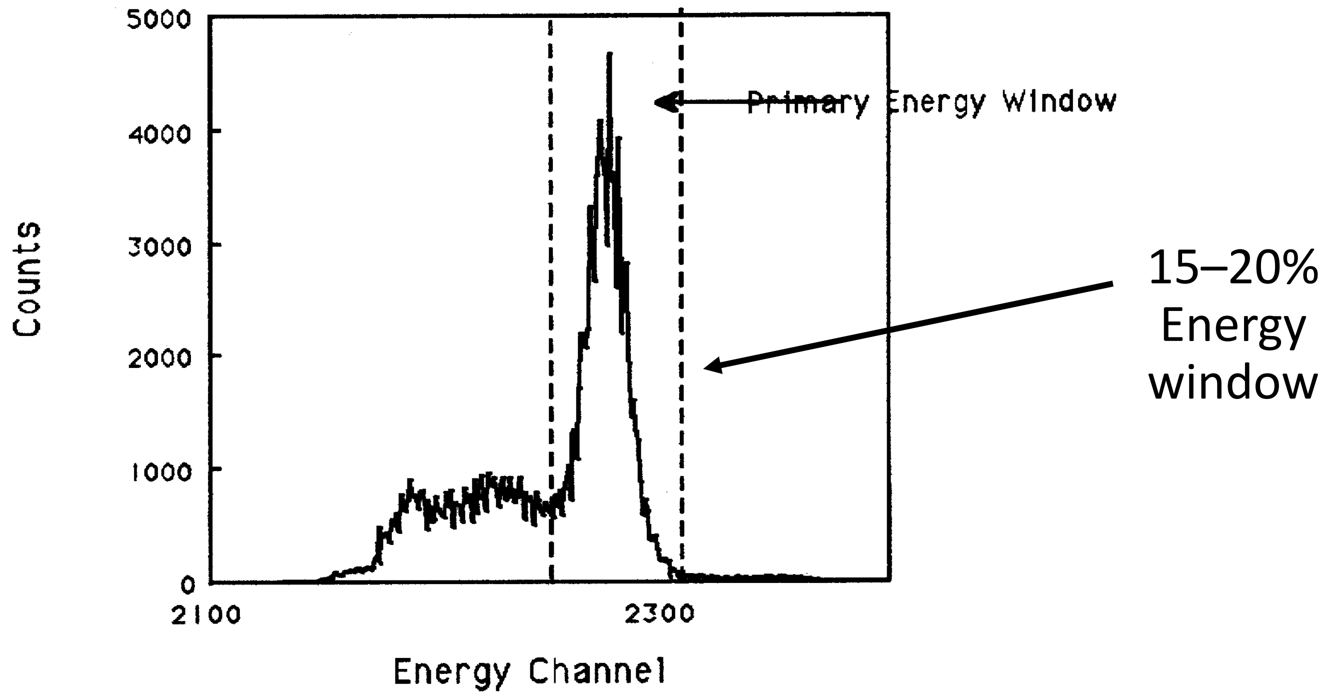

Typical Anger camera has from 8–10% FWHM energy resolution at 140 keV

Detector Technology for Improving Spatial Resolution – Discrete Detector Elements

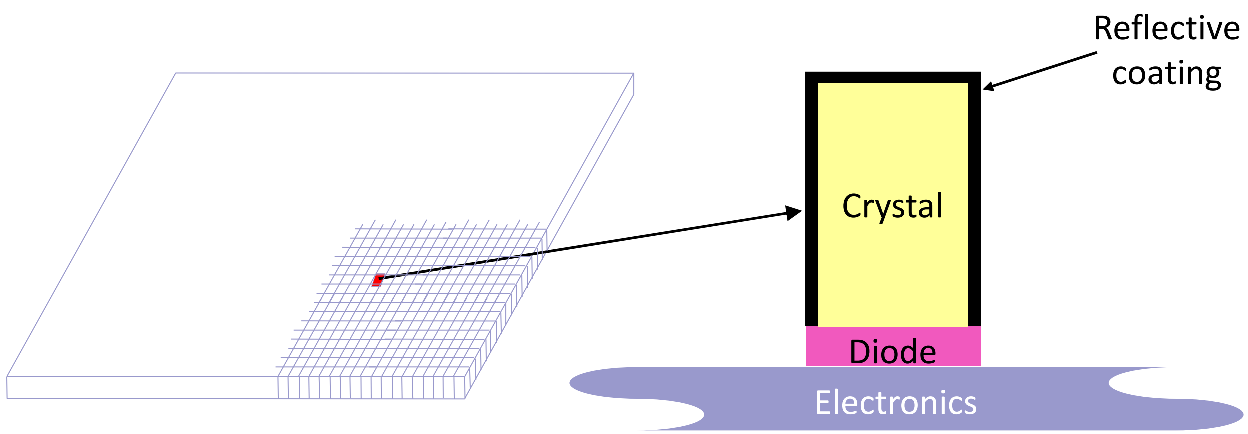

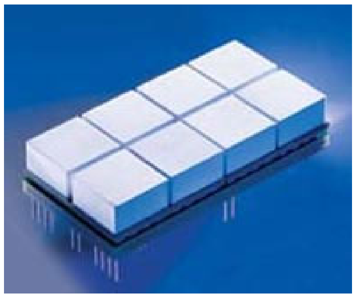

Eight modules in array

- Pixellated CsI(Tl) scintillator separated by reflector
- Arrays of PIN photodiodes and readout electronics

Drawing courtesy Jerome Gormley, Digirad, Inc

Comparing HPGe and Room Temperature Semiconductor Materials

Detector Material	Z	E_G (eV)	E_{pair} (eV/ehp)	Density (g/cm3)	Resitivity @ 300K (Ω·cm)	$\mu\tau_{e/h}$ (cm^2/V)	Knoop Hardness
Ge	32	0.66	2.9	5.33	50	>1/>1	
Si	14	1.12	3.6	2.33	~10^4	>1/~1	1150
CdTe	48/52	1.4	4.4	6.2	10^9	10^{-3}/ 10^{-4}	45
CdZnTe	48/30/52	1.6	4.7	~6.2	10^{11}	10^{-2}/ 10^{-4}	
HgI_2	80/53	2.1	4.2	6.4	10^{13}	10^{-2}/ 10^{-4}	<10
GaAs	31/33	1.4	4.3	5.32	10^8	10^{-5}/ 10^{-6}	
Diamond	6	5	13	3.51	>10^{13}	10^{-5}/ 10^{-5}	10000
TlBr	81/35	2.7	5.9	7.56	10^{11}	10^{-5}/ 10^{-6}	
InP	49/15	1.4	4.2	4.78	10^7	10^{-5}/ 10^{-5}	

In semiconductor: total signal generated: ~22,700 → much smaller statistical fluctuation compared with that for scintillator!!

Further helped by the Fano factor (Please see the definition on page 115 and typical value for semiconductor on page 357, both on G. F. Knoll's text)

The HEXITEC Detector

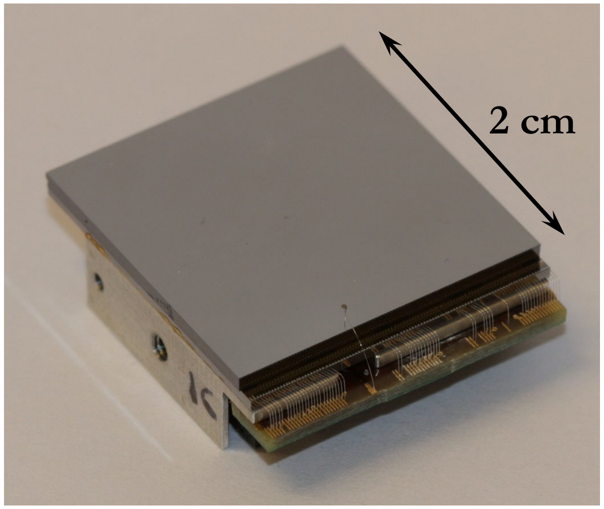

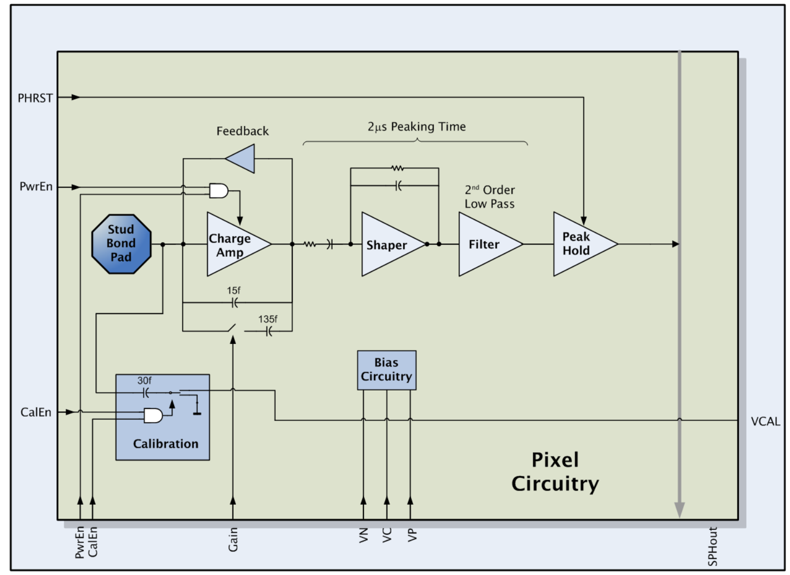

The HEXITEC detector

Pixel readout circuitry

- Modular, 2 cm x 2 cm, 3-side butterable.
- 80x80 channels on 250μm pitch.
- 9000 f/s with 4 80x20 Quadrants Readout Simultaneously
- Low noise measurement of charge deposited to get good energy resolution.
- Readout energy on each pixel and, off-chip, build up spectrum per pixel over many frames.
- CdTe, 1-2mm, CZT, 2-5 mm thickness

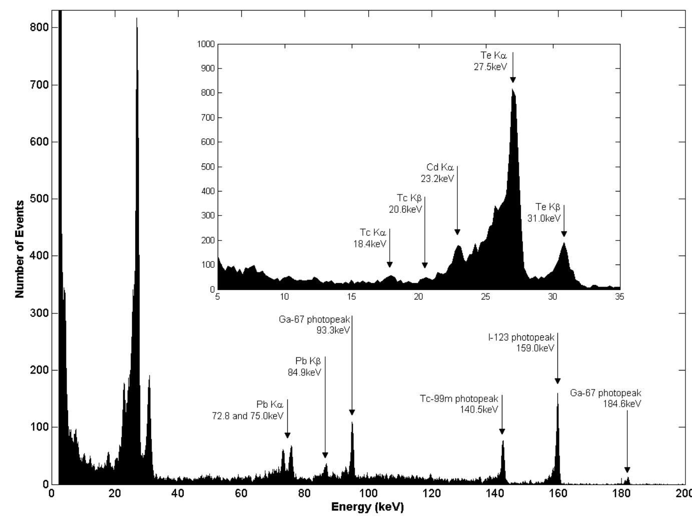

Figures and text from Matt Wilson and Paul Seller, Rutherford Appleton Lab, UK, STFC.

Hybrid Pixel-Waveform CZT and CdTe Detectors

Pixel readout circuitry to provide
- Pixel address
- Coarse timing info for synchronizing the cathode and anode readout operation
- Coarse energy information (if needed)

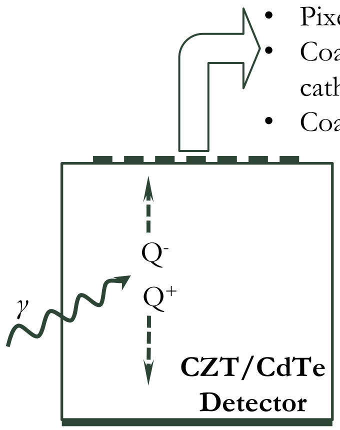

Waveform sampling circuitry to provide
- Precise timing
- Accurate depth of interaction (DOI) information
- Energy information

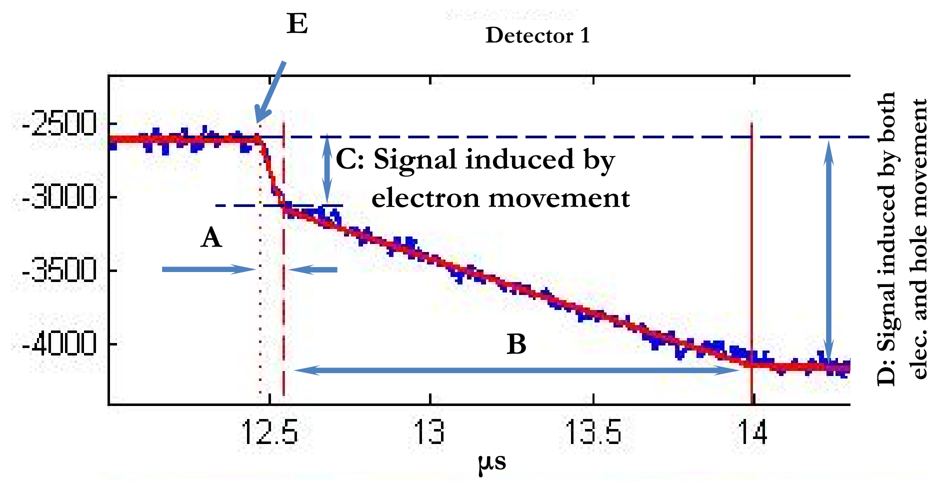

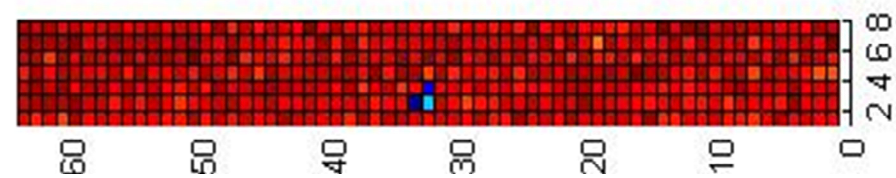

The **Shockley–Ramo theorem** states: The charge Q and current *i* on an electrode induced by a moving point charge q are given by:

$$Q = -q\varphi_0(\boldsymbol{x})$$

$$i = q\boldsymbol{v} \cdot \boldsymbol{E}_0(\boldsymbol{x})$$

where $\boldsymbol{v}$ is the instantaneous velocity of charge q. $\varphi_0(\boldsymbol{x})$. and $E_0(\boldsymbol{x})$ are called the **weighting potential** and the weighting field, respectively.

Z. He et al, NIM A380 (1996) 228, NIM A388 (1997) 180.

Benefits (presented at **IEEE RTSD 2011 and Meng, NIM 2005, 2006, Groll et al., IEEE TNS 2016**):

- Highly simplified pixel-circuitry, pixel address and triggering only.
- Improved timing and DOI resolution (for single interaction).
- Independent of anode configurations – allow the use of further reduced pixel sizes and therefore further improved spatial resolution.

Small-Pixel Semiconductor Detectors

Is this the solution for future ultrahigh resolution nuclear imaging systems?

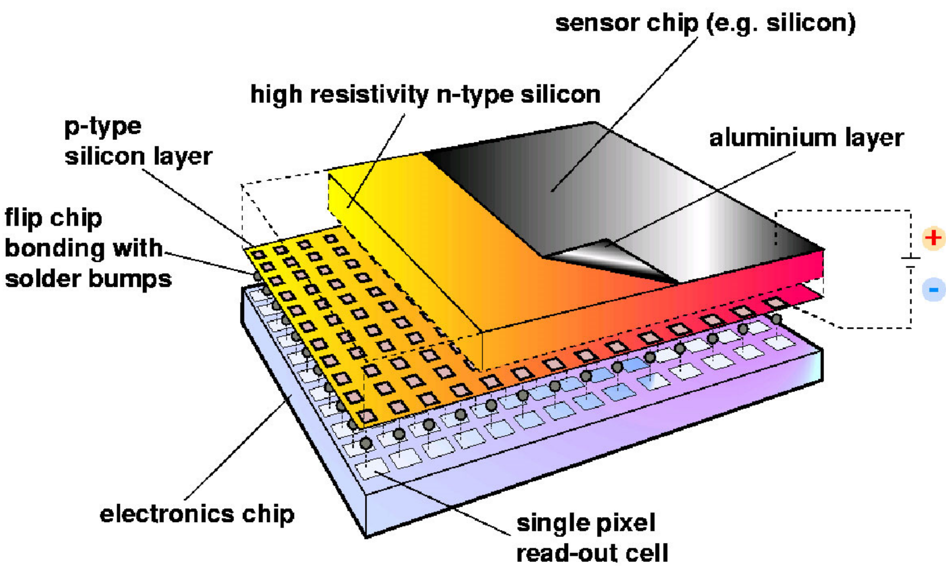

Medipix II hybrid pixel sensor

M. Campbell, V. Rosso, IEEE NSS-MIC 2004 Conference Record.

Not quite …

- Energy resolution affected by incomplete charge collection.
- DOI resolution is either unavailable, or relatively poor.
- Timing information is limited by the slow charge drafting in semiconductor.
- Count rate capability MAY be limited by the complexity of the readout system.
- A single detector capable for both PET and SPECT is not available.

The UIUC ERPC Detector: Different Variations

FPGA for controlling the readout sequence

Detector hybrids
1.1 cm × 2.2 cm

Wire-bonding to the readout PCB

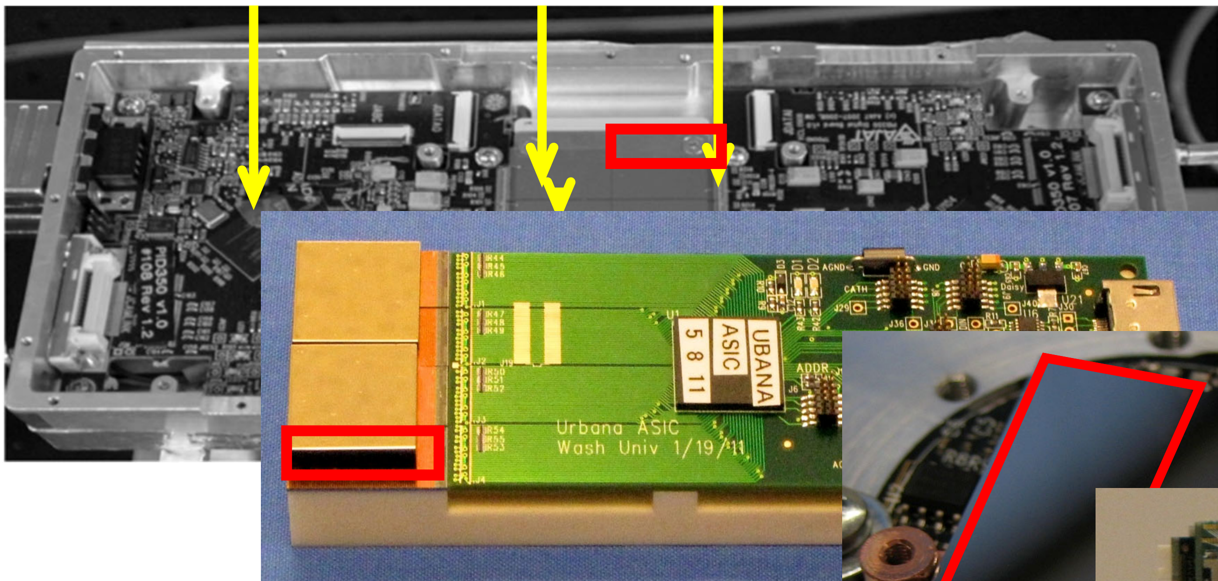

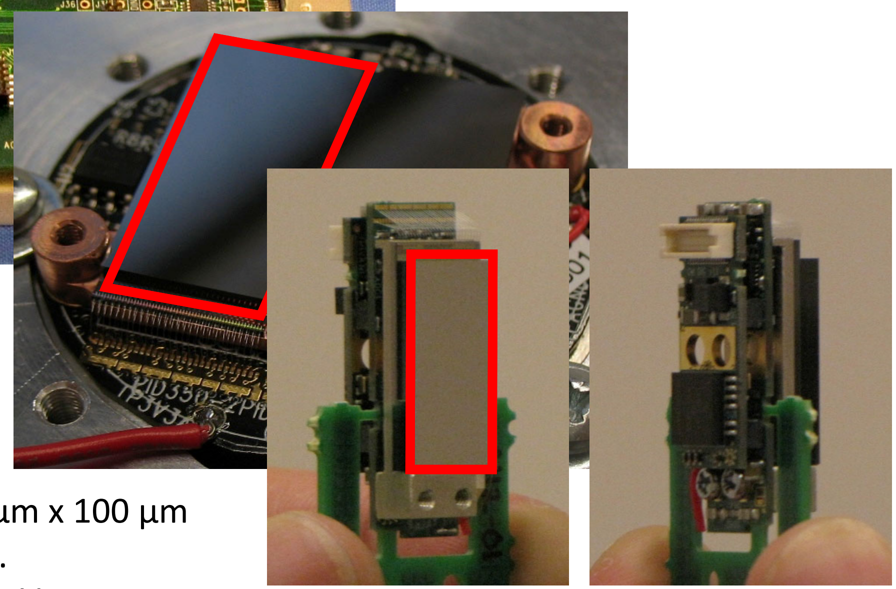

2006 – 2017

On the same detector:

- Spatial resolution in 3D: 350 μm x 2 mm (depth) → 100 μm x 100 μm
- Energy resolution: 3-4 keV (30-200) → 1 keV (5-200 keV).
- Dynamic range: 30-600 keV → 5-200 keV and 60 keV-2MeV.
- Improved effective sensitivity from precisely determined interaction patterns.

On-going Development of a Large-Area Deformable 3-D HEXITEC Detector Platform

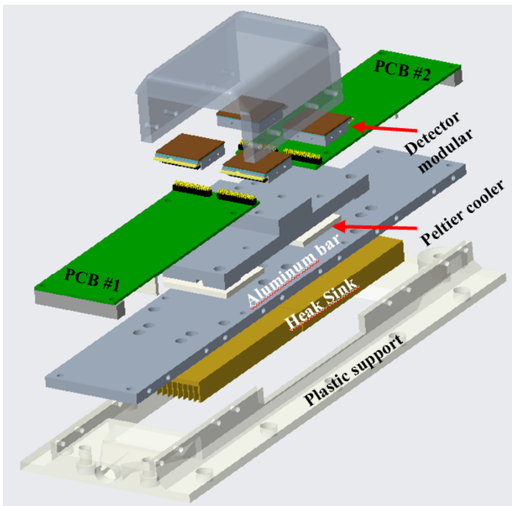

Key modifications:

- **Self-contained modular** design to allow flexible sensing areas.
- **On-board processing** to minimize the data rate to be sent to the DAQ system.
- **Flexible cables** (USB-C/optical, power, trigger in/out) to connect to a mother board.
- Add-on-board for **DOI readout**.

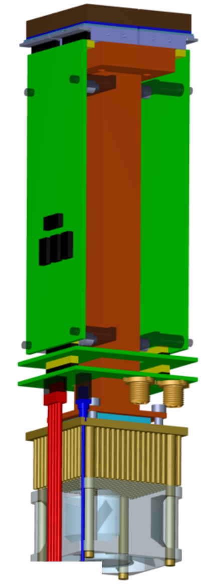

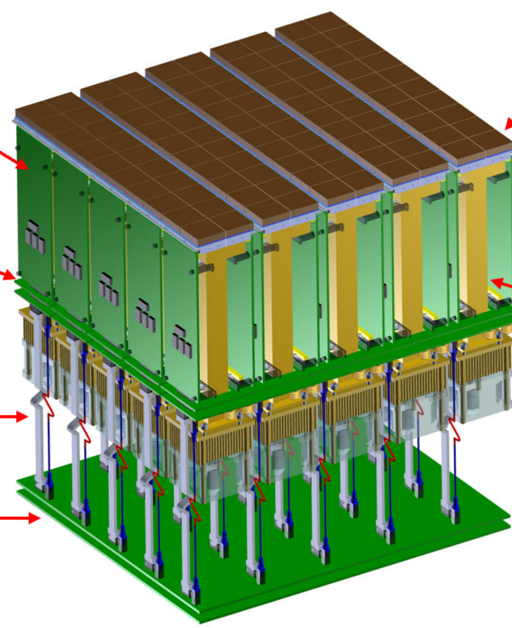

SIEMENS CZT “CASSETTE” (12 cm x 20 cm)

Courtesy Doug Wagenaar, Siemens Medical Solutions

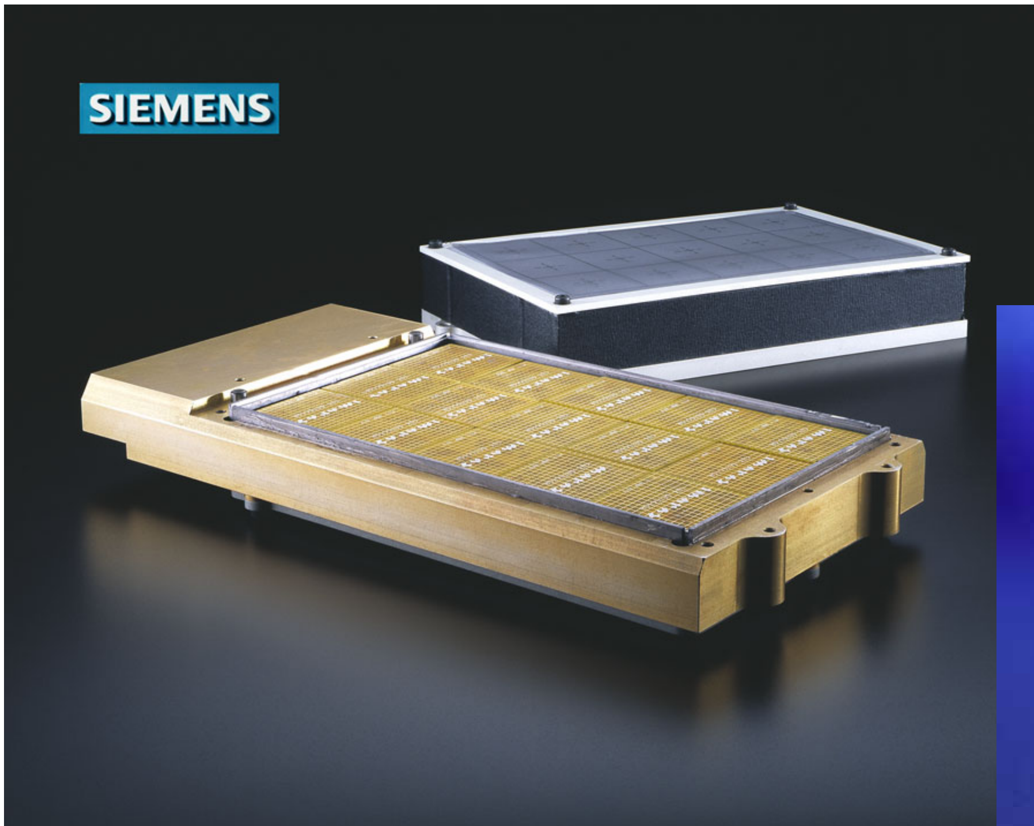

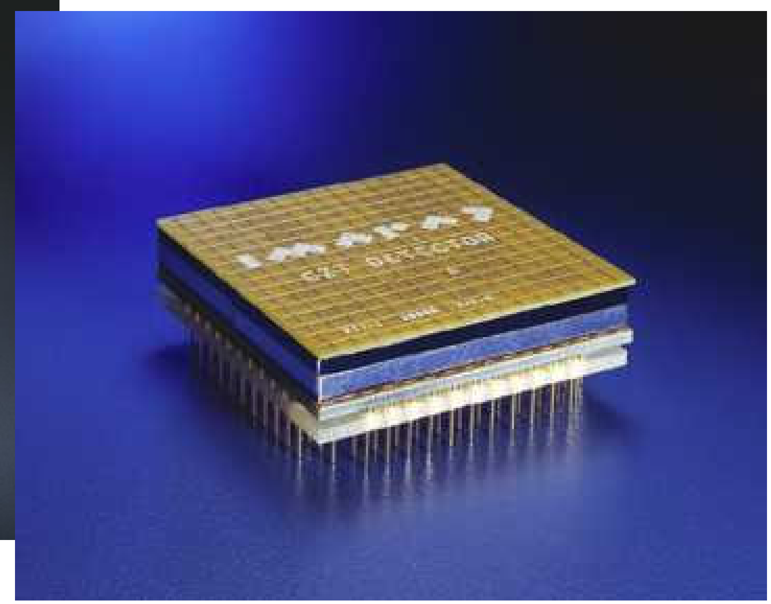

Works-in-progress prototype, not available as a product.

Scintillation Crystal Properties

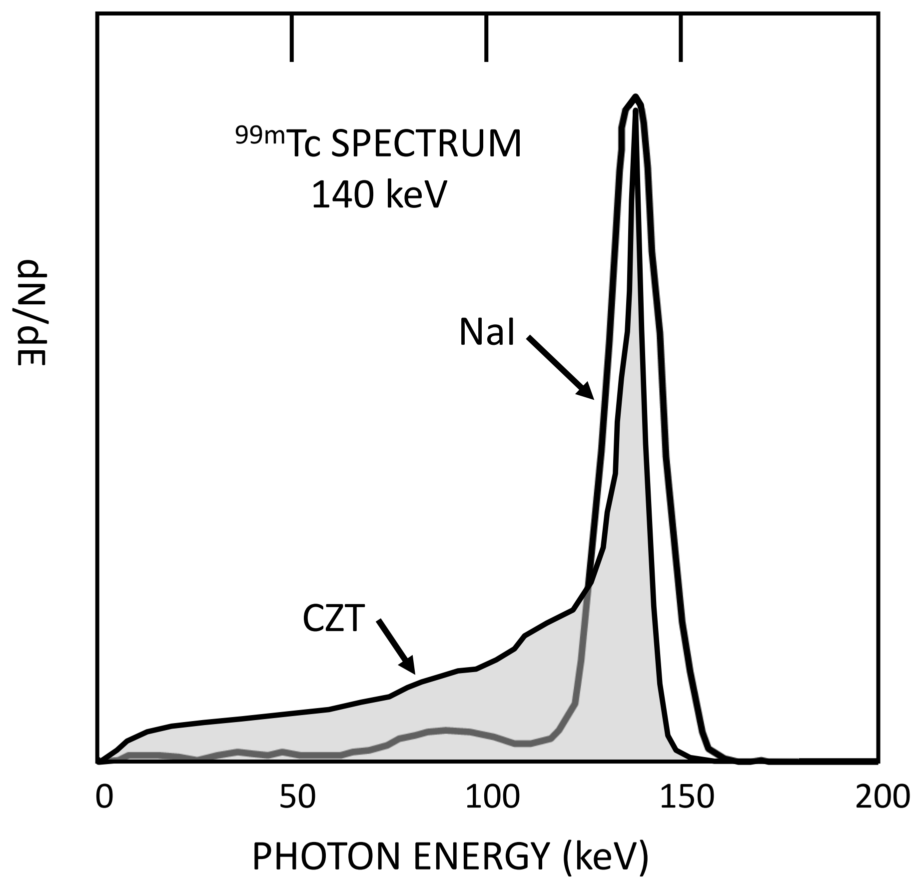

^{99m}Tc intrinsic (non-collimated) spectra obtained with CdZnTe (CZT) and NaI(Tl) detector systems. Note the low energy "tailing" of the CZT, and the 110 keV escape peak in the CZT spectrum.

Courtesy Doug Wagenaar, Siemens Medical Solutions

We are not quite there yet in terms of the achieved energy resolution. But the benefit in overall image quality is already significant!

Charge-Sharing Correction that Incorporates the Correlations between the Responses of Adjacent Pixels

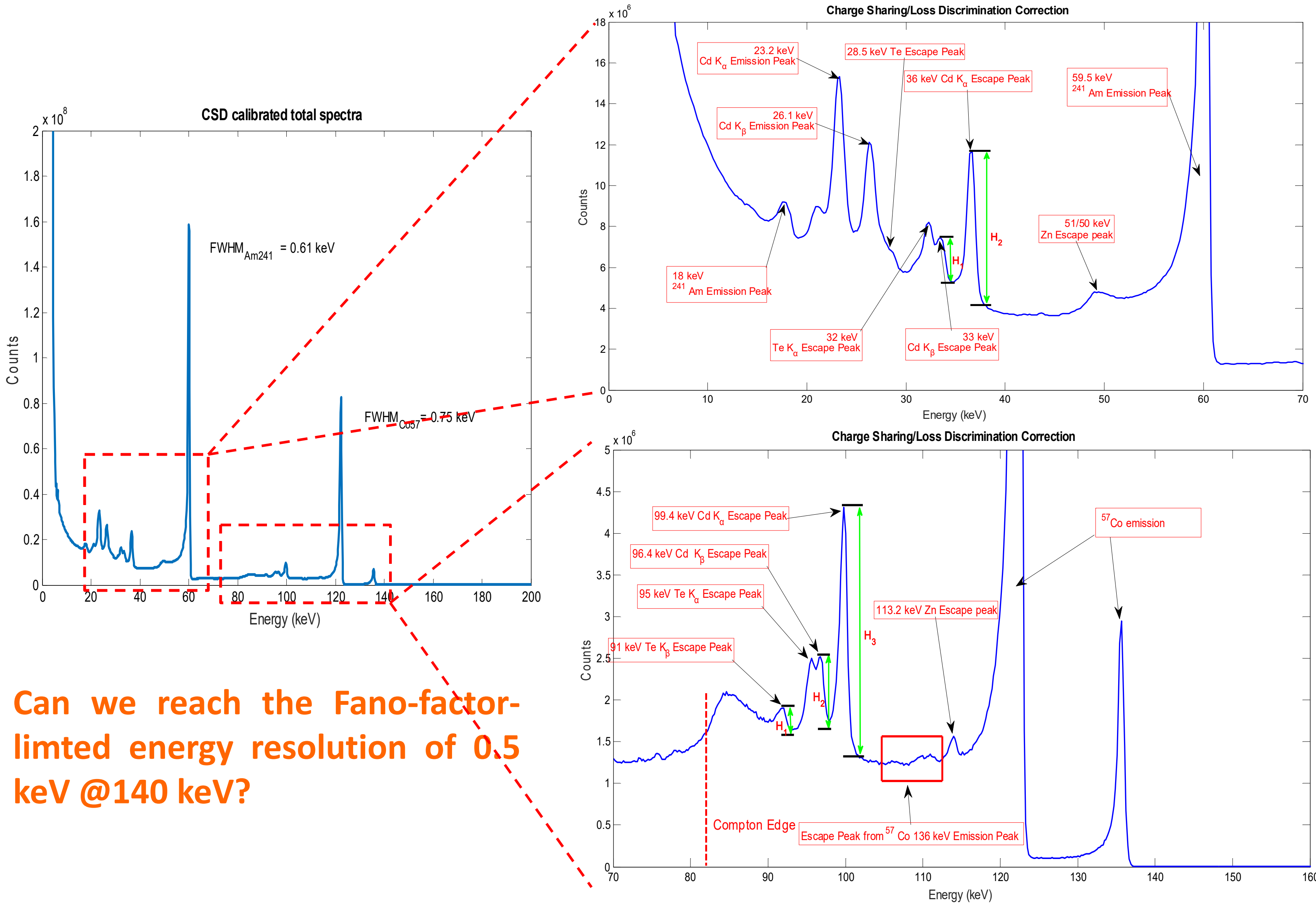

Can we reach the Fano-factor-limted energy resolution of 0.5 keV @140 keV?

4 radioisotopes

0.1 mL each/0.25 mCi
(Tc99m,Tl201,I123,In111)
4 vials of 250 uL, parallel to set surface
1 hr at 800 fps
No Scattering media

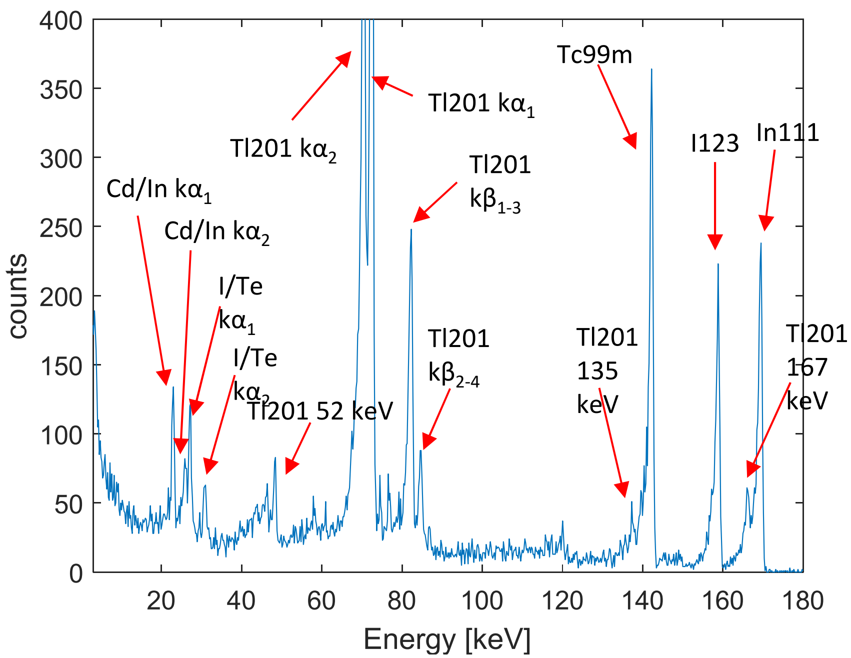

Energy resolution obtained with all 6400 pixels on a 2 cm x 2 cm CdTe detector

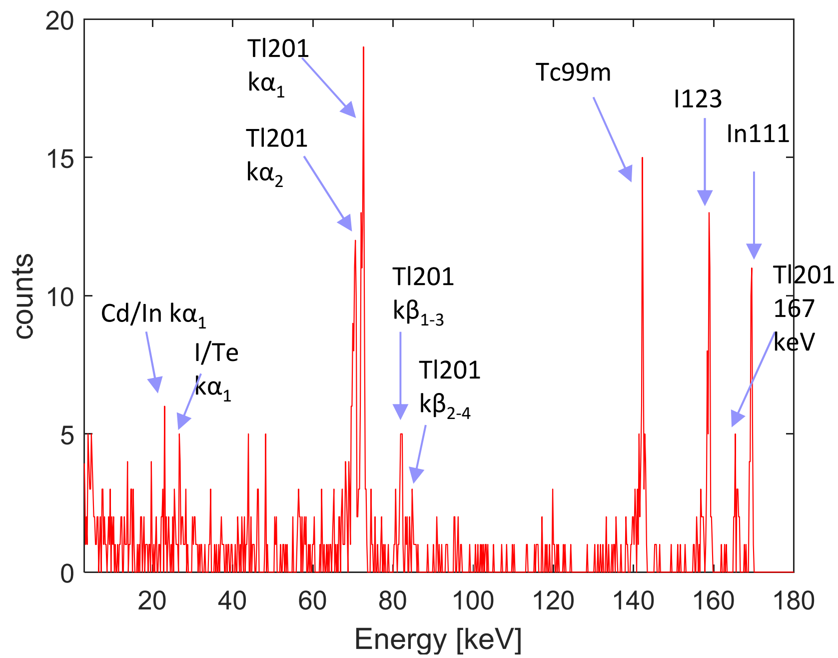

Energy resolution obtained on a single pixel

Controlled Charge Collection

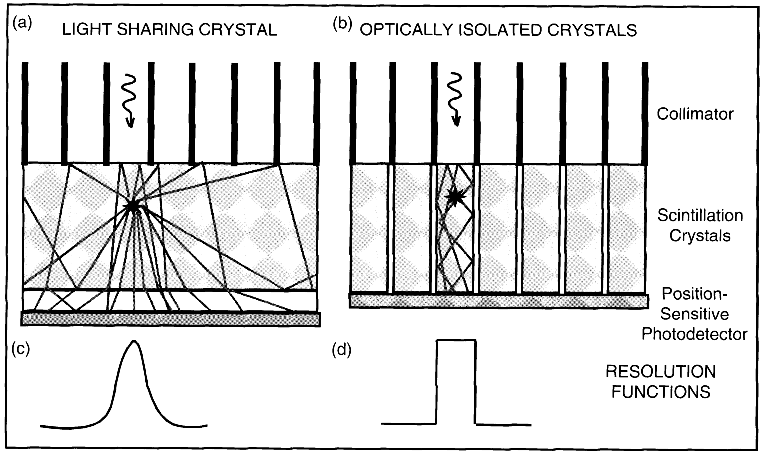

FIGURE 6 Schematic drawings of the light ray propagation for typical (a) single and (b) multiple scintillation crystal camera designs. For the pixellated design, scintillation light is confined to one crystal and focused on one spot of the photodetecting array. (c,d) Approximate shapes of the resulting theoretical intrinsic point spread functions for single-photon imaging.

Collection of visible photons in scintillator

Apply electric field to drive the charge carriers

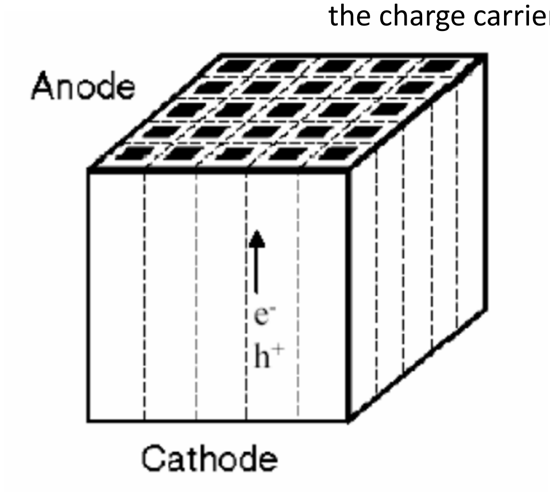

Collection of charge carriers in semiconductor

In semiconductor, electron and holes are driven by electric field.

Spatial spreading of the charge carriers can be better controlled, so that a better spatial resolution can be achieved.

A Typical Measured Energy Spectrum

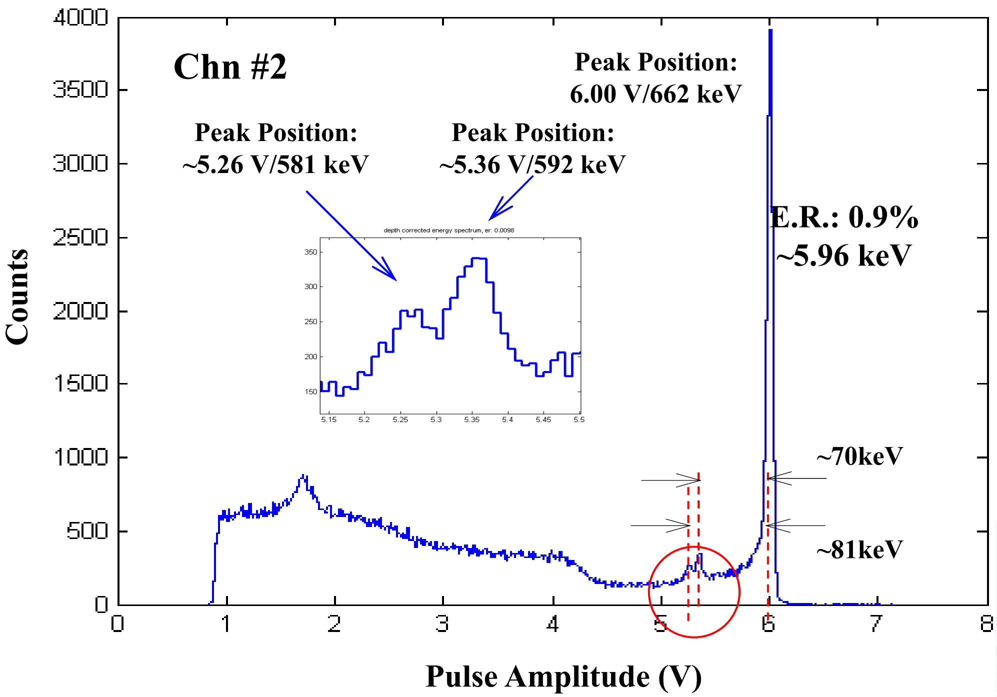

Measured energy spectrum from HgI_2 semiconductor, 1mm thick, 1x1mm^2 pixels

Typical energy spectrum from a 3 inch NaI(Tl) scintillation counter

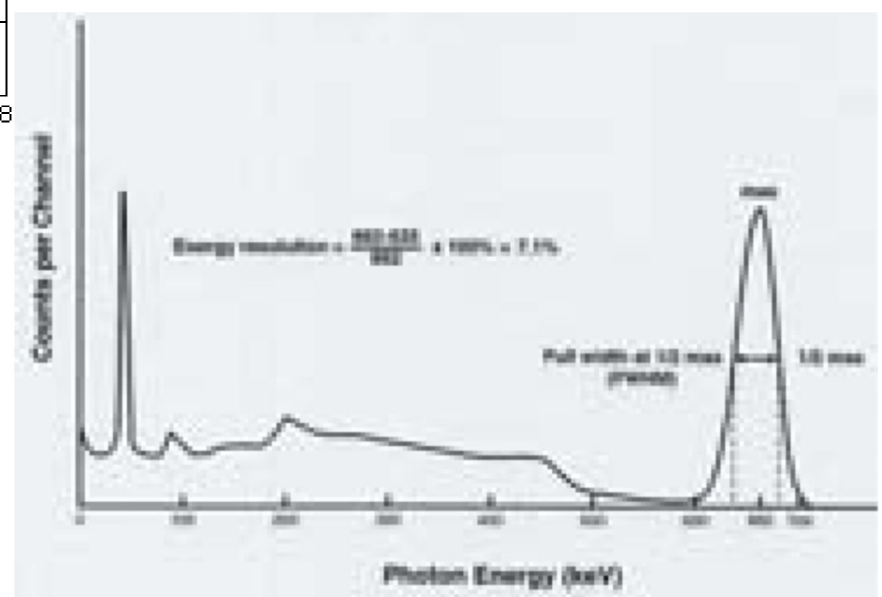

Comparing Co-60 Spectra Measured with NaI(Tl) and HPGe Detectors

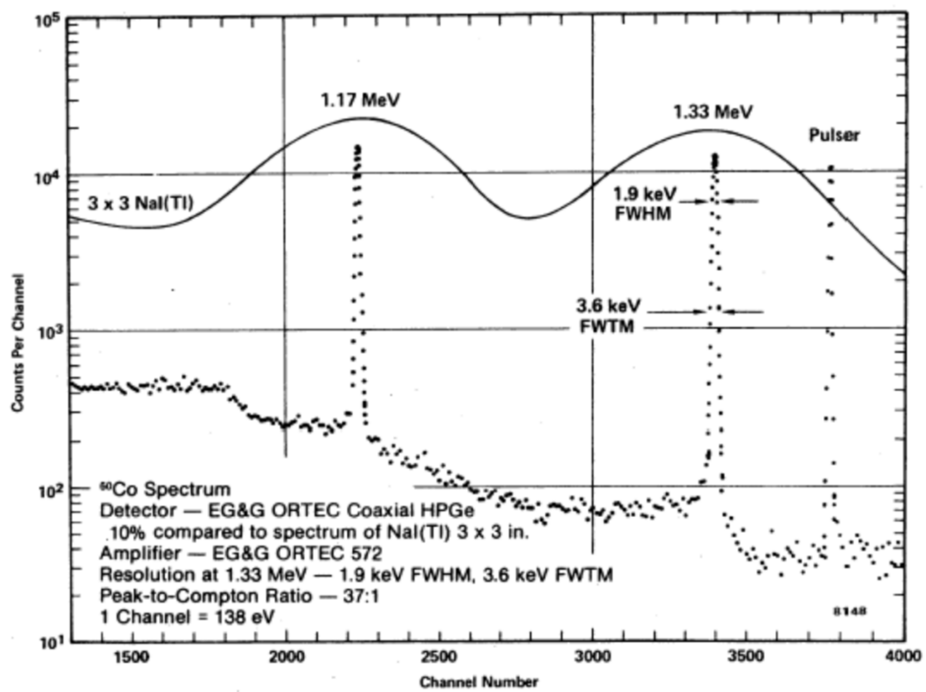

One of the major advantages of semiconductor detector is the improved energy resolution ..

NaI versus CZT Comparison

NaI

CZT

SIEMENS CZT CASSETTE

Courtesy Doug Wagenaar, Siemens Medical Solutions

Brain Images

NaI Mosaic CZT

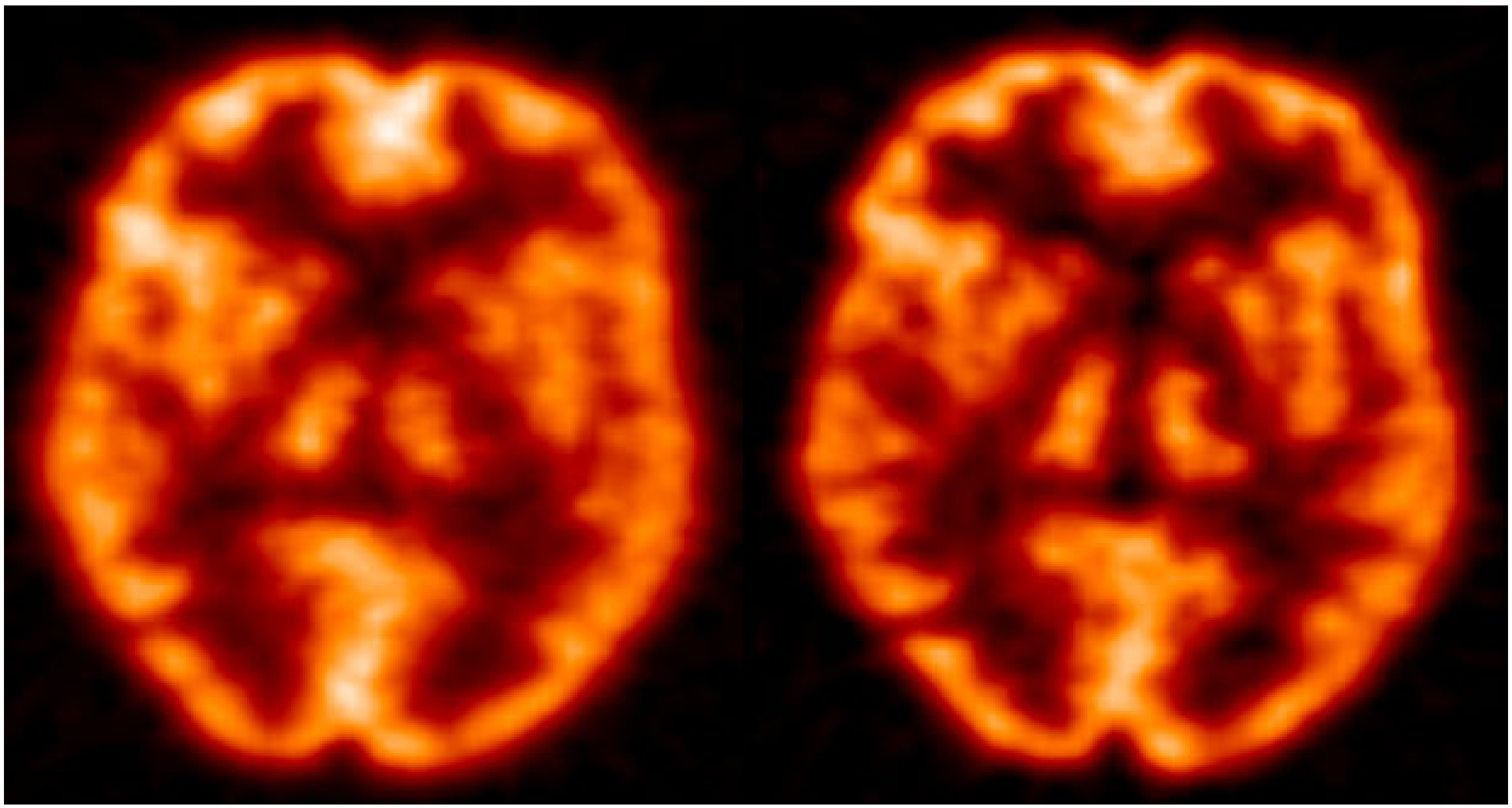

Improved Image Quality

SPECT Basics

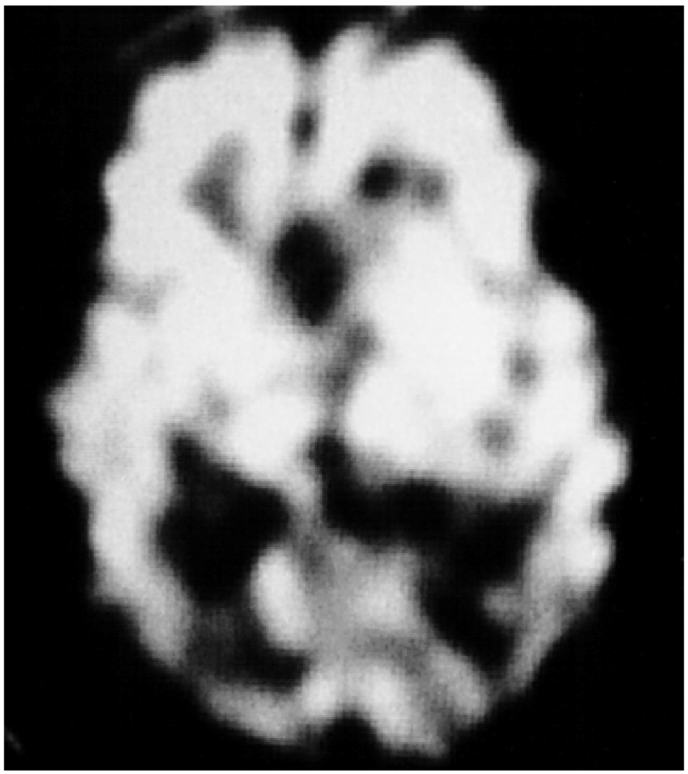

- Sensitive to:
  Tracer (Drug) Concentration
- Contrast:
  Tracer vs. No Tracer
- Advantages:
  + Visualizes Metabolism
  + Acceptable Imaging Time
- Disadvantages:
  – Ionizing Radiation
  – Low Resolution

Basic SPECT – Projection Data

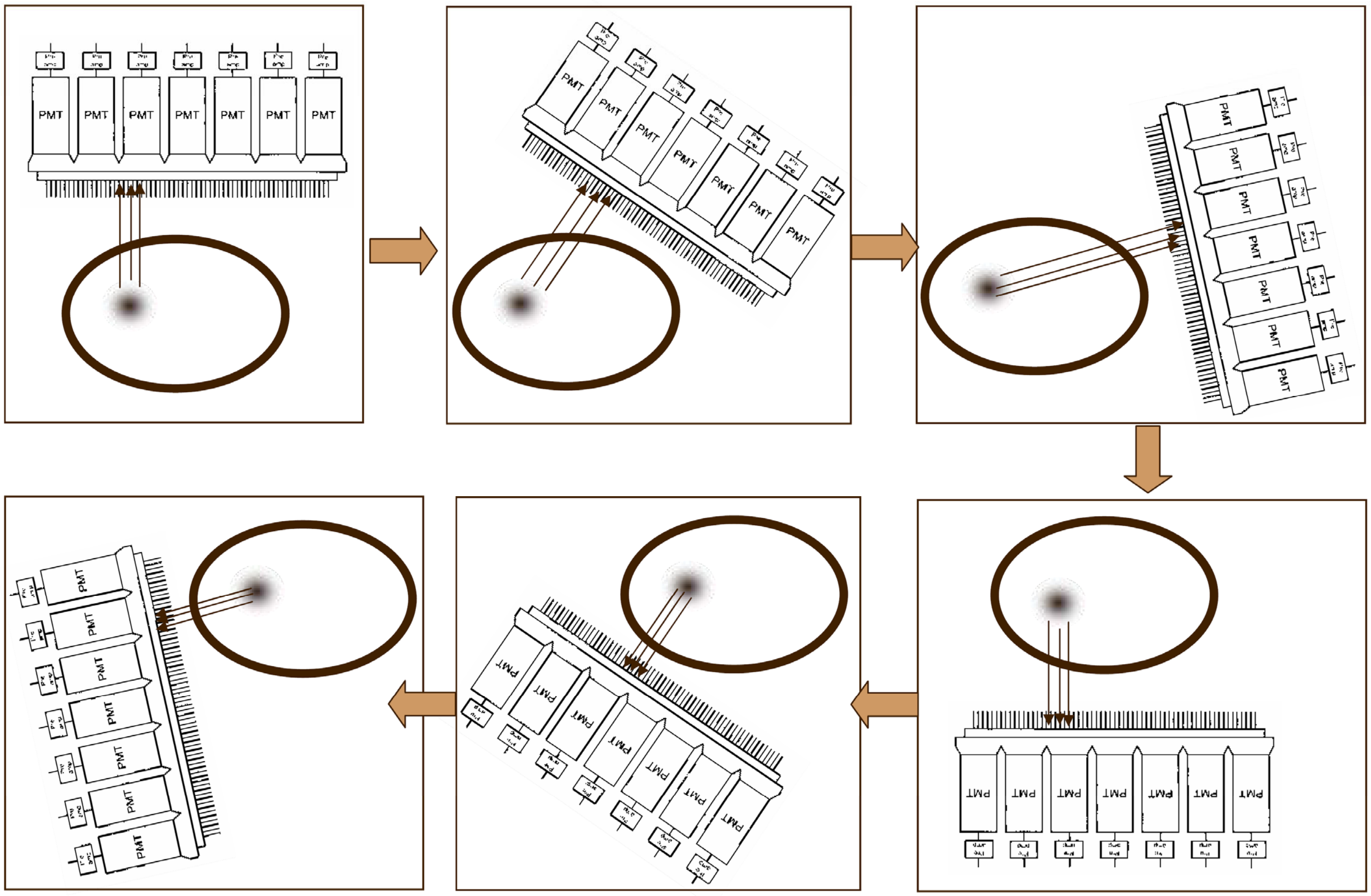

Early Clinical SPECT

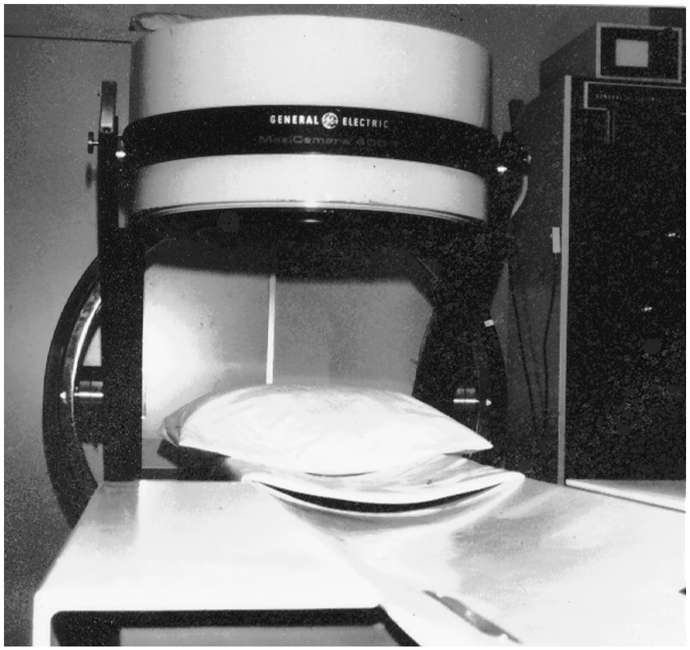

The First Anger Camera

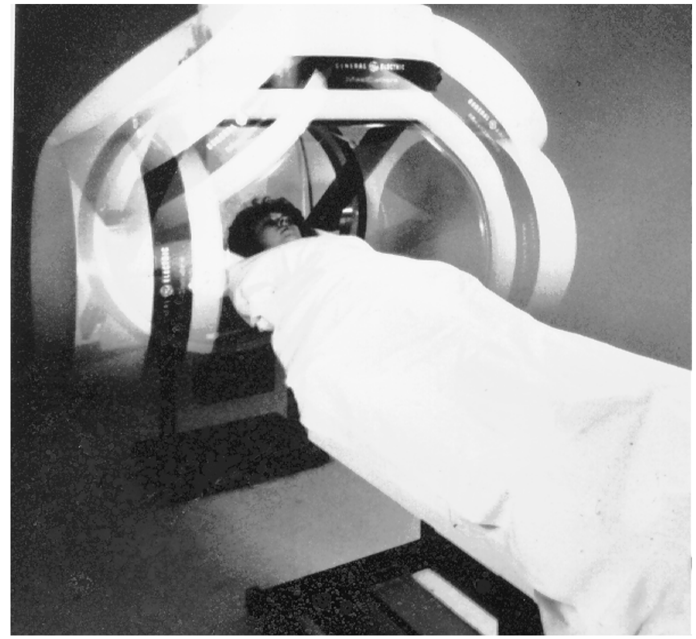

GE 400T Rotating Anger Camera (ca. 1981)

Modern Clinical Systems

GE Millenium VG

Philips Cardio 60

Siemens e.cam
Variable Angle